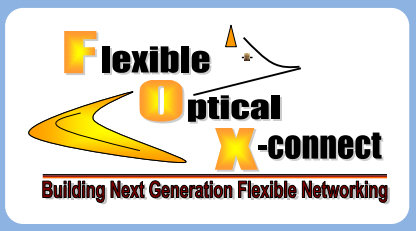

PROJECT: **FOX-C** CONTRACT NO.: **318415**
FLEXIBLE OPTICAL CROSS-CONNECT NODES
ENABLING NEXT-GENERATION FLEXIBLE OPTICAL NETWORKING

Specific Targeted Research Project (STREP)
Information & Communication Technologies (ICT)

Document Type: Deliverable

Dissemination Level: RE

D2.2

Flexible system emulation platform and report on its performance evaluation

Lead beneficiary:	Tyndal/UCC, AIT
Contact person:	Jian Zhao (Tyndall/UCC), Dimitrios Klonidis (AIT)
Address:	Tyndall National Institute and University College Cork, Lee Maltings, Dyke Parade, Cork, Ireland Athens Information Technology Centre, 0.8km Markopoulou Av., 19002, Peania-Attika, Greece e-mail: jian.zhao@tyndall.ie; dikl@ait.gr;

Date due of delivery:	31/03/2014
Submission date:	27/06/2014
Contributing institutes:	Tyndall/UCC, ASTON, AIT, HUJI
Authors:	Jian Zhao (Tyndall/UCC), Stylianos Syngletos (ASTON), Dimitrios Klonidis (AIT), Dan Marom (HUJI), José M. Rivas (AIT)

This deliverable reports on the design and back-to-back performance of the different transmitter-receiver models under evaluation in WP3 as well as the description of the switching node configurations with ultra-fine granularity add/drop functionalities discussed in WP4 alongside the performance analysis of the transceiver-node pair and the effect of transmission through routes with one flexible OADM node.

Revision History

No.	Version	Author(s)	Date
1	0.1	Dimitrios Klonidis (AIT)	**28/02/14**
	Comments:	**Initial template and table of contents**	
2	0.2	Jian Zhao (Tyndall-UCC)	**25/03/14**
	Comments:	**Revised version with the Tyndall inputs**	
3	0.3	Jian Zhao (Tyndall-UCC)	**29/03/14**
	Comments:	**Second version**	
4	0.4	Dimitrios Klonidis (AIT), Jian Zhao (Tyndall-UCC)	**30/03/14**
	Comments:	**Revised version with AIT's inputs**	
5	0.5	José M. Rivas (AIT), Stylianos Syngletos (ASTON) Jian Zhao (Tyndall-UCC)	**17/06/14**
	Comments:	**Revised version, including inputs from ASTON and revisions by AIT and Tyndall-UCC.**	
6	1.0	José M. Rivas (AIT), Dimitrios Klonidis (AIT)	**27/06/14**
	Comments:	**Final revision and submission of deliverable**	
7			
	Comments:		
8			
	Comments:		
9			
	Comments:		
10			
	Comments:		

Table of Contents

List of Figures

List of Tables

Executive Summary

The FOX-C project aims at enabling the end-to-end network routing of any tributary channel with flexible bandwidth down to 10Gb/s carried over a super-channel with an aggregated capacity of at least 1Tb/s. This is possible through the design, development and evaluation of flexible switching nodes with fine switching granularity, as well as the adoption of flexible transmission solutions compatible with the FOX-C switching concept.

Super-channels can be regarded by the network nodes both as an autonomous high capacity end-to-end channels and as a channel carrying a group of flex-channels with common characteristics, thereby defining two switching levels: a coarse switching level that handles the whole super-channel as one high capacity channel and a fine switching level that handles the individual contents of the super-channel.

In this deliverable, drawing on the work carried out in work packages 2, 3 and 4, we focus on the key technology solutions and the requirements for both the flexible transceiver and the flexible switching subsystems. With regard to the flexible transceiver design options, two optical multiplexing schemes —namely the Nyquist-WDM and the optical OFDM techniques— and three electrical schemes —electronic OFDM (eOFDM), electronic fast OFDM (eFOFDM) and Nyquist-FDM— are examined for the creation of the super-channel. On the other hand, with regard to the design of the FOX-C node, two novel filtering and switching subsystems allowing the transparent handling (add, drop and pass-through) of low-rate channels directly from the ultra-high capacity super-channel have been investigated. In this respect, we present the design characteristics and specifications of a high spectral resolution adaptive filter compatible with multi-carrier signals without overlapping spectra and a solution based on an interferometric architecture that performs channel erase (clearing) and addition of a new channel with capability to be used with all types of multiplexed multi-carrier signals.

Building on the design and specifications for the electronic transceiver and the high-spectral-resolution-filter-based switching models discussed above, the system performance is investigated through simulation to determine the optimal design parameters and the penalties imposed by the filtering (both at the transmitter, to pre-shape the channel, and at the receiver, to select it) and the transmission when high-order quadrature modulation formats and coherent detection are employed. N-FDM proved to be the solution with the weakest performance in terms of BER vs. OSNR due to the impossibility to create a sufficiently sharp electronic filter at the transmitter to account for the overlapping nature of this type of signal in the time domain.

From the results of the transmission studies carried out for the high spectral resolution filter, we extracted the required specifications that guarantee an appropriate performance of a super-channel based on eOFDM and eFOFDM. Despite the aforementioned incurred penalty for N-FDM, this technology achieved a more stable performance when the guard interval of the eOFDM and eFOFDM solutions was reduced below a minimum length that prevented dispersion from being fully compensated at the digital processing stage of the receiver.

1 Introduction

This chapter provides an introduction to the simulation work carried out in T2.2 for the characterization of the flexible node subsystems in the FOX-C project and presents a summary of the cases studied and the methodology used with a view to providing the reader with a comprehensive picture of the structure of the document and the results that can be found in it.

1.1 Purpose of the system modelling studies and targets

Following up the work carried out in T2.1 to do with the definition and specifications of the reference flexible optical communication system in the FOX-C project as well as the developments regarding the flexible transmission schemes in T3.1 and T3.2 and the flexible node designs in T4.3 and T.4.4, the purpose of T2.2 has been to develop the appropriate component and system level models in order to define theoretically the performance characteristics of the solutions proposed and developed in WP3 and WP4.

Initially T2.2 ran in parallel to T2.1, from which it received the system definitions required for the development of the models. Then the theoretical models for the transport and node subsystems were updated with the technical data and design specifications received as feedback from WP3 and WP4.

The system model platform developed in T2.2 serves a threefold purpose:

- By varying certain design characteristics, the system model platform allows examining the system tolerances for the various solutions in terms of the transmission and switching impairments.
- It can provide feedback to WP3 and WP4 indicating the design characteristics of the subsystems that require particular attention.
- It offers a powerful and accurate tool for the overall system performance evaluation studies in T2.3 leading to the identification of the operating limits of a flexible network incorporating the FOX-C solutions with the ulterior aim of analysing the benefits of such a network in terms of power consumption and cost saving.

This document reports on the expected system performance, based on simulation results, due to the tolerances of the different design parameters, and informs of the effect that their degree of variability has on the overall system performance.

1.2 Reference to flexible multiplexing schemes defined in the FOX-C project

The FOX-C project targets the development of a flexible switching node with ultra-fine switching granularity providing the capability to drop and add low-rate tributaries (defined as “flex-channels”) directly from/to an ultra-high capacity channel (defined as a “super-channel”).

The flexible node of the FOX-C project is an advanced version of ROADM able to add, drop and pass-through low-granularity flex-channels extracted from and added to super-channels. This is addressed in a hierarchical topology (see Figure 1.1), providing the following functionality:

- At the **fibre link level**, a WSS can select one super-channel that contains the flex-channels to be dropped locally. The rest of the super-channels continue directly to the output port. Up to this point the function of the node is similar to a typical WDM ROADM but with a finer adaptation to a variable spectral range and not to a fixed grid (e.g. 100GHz or 50GHz band) as in WDM systems.

- At the **super-channel level**, a distinction has to be made between the drop and the add sections of the FOX-C node:
  - At the **drop section**, the extracted super-channel is subdivided into flex-channels for either drop or express pass-through. This differs from the conventional spectral filtering used for WDM channel processing on account of the overlapping properties of the orthogonal subcarriers in the frequency domain for the case of OFDM or the inability to provide sharp edge filtering for the case of Nyquist FDM.
  - At the **add section**, the newly inserted flex-channels are either coupled and then processed by a phase synchronization and regeneration stage in the case of optical OFDM or first spectrally pre-shaped and then coupled with the through-bands for the case of Nyquist WDM.
- At the **band/channel level**, the dropped flex-channels destined to the metro/access network segment are either expressed transparently to the lower segment of the system for processing at the access terminal nodes or coherently detected with the appropriate Nyquist FDM or OFDM receivers and processed with common low rate switching elements (e.g. DXCs). Similarly, at the add interface the Nyquist FDM or OFDM encoded tributaries are fed to the FOX-C node either directly from the metro/access segments or from the edge switches.

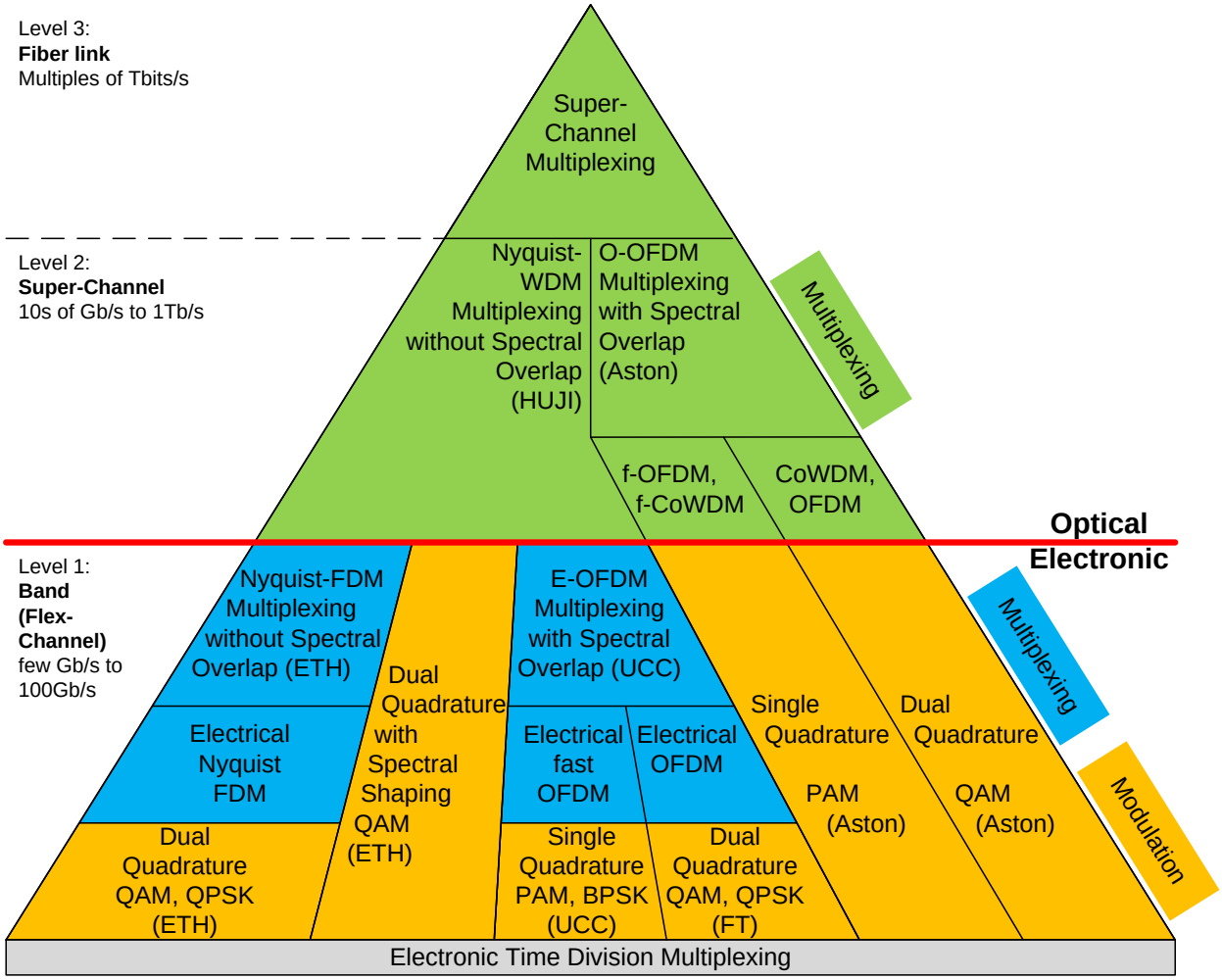

Figure 1.1 – Overview of optical multiplexing schemes investigated in FOX-C (in green), electrical multiplexing schemes (in blue) and the targeted modulation formats (in orange).

Since the FOX-C project adopts two switching levels in the optical domain, the maximum switching granularity is defined by the maximum spectral width and aggregated data rate that can be assigned to a

super-channel, and the minimum switching granularity is defined by the smallest spectral width and data rate of a single flex-channel. Because the FOX-C project targets solutions applicable to the core network (extended to metro segments) a targeted minimum granularity of 10Gb/s has been defined. The maximum granularity is determined by the operating standards. ITU-T SG 15 has been considering "beyond 100G" solutions for a few years now and appears to be moving towards the standardisation of a new OTU5 (supporting line rates of probably 400Gbps) or/and an OTUadapt with flexible rates running into at least 1Tbps; the recently created IEEE P802.3bs Task Force has been chartered with the development of the IEEE P802.3bs 400 Gigabit Ethernet (GbE) project; and OIF has recently started to work on a 400G Framework Document to analyse and discuss tradeoffs among high-order modulation formats, high data rates per channel and number of subcarriers for long-haul and metro applications. Therefore it is clear that the maximum granularity of the node is required to be at least 400Gbps or even 1Tbps. The FOX-C target for this level is set to beyond 1Tb/s and intends to investigate capacities up to 4Tb/s per super-channel.

1.3 Cases studied

In T2.2, two all-optical and three electronic transceiver configurations have been investigated to carry out the performance characterisation of the flexible node subsystems. In this document we report the results of this investigation.

The document is structured as follows. First, in chapter 2, the different transmitter-receiver models are taken into consideration. The set-up and design parameters of all optical and electronic schemes are presented. We analysed all-optical OFDM (AO-OFDM), Nyquist WDM (N-WDM), electronic OFDM (eOFDM), electronic fast OFDM (eFOFDM) and Nyquist FDM (N-FDM) in turn. In the case of the all-optical schemes, the parameters presented are those being used in the experimental implementations in WP3 and will be updated if need be in a revised version of this document to be submitted later this year.

For the electronic schemes, the back-to-back performance of a single optical channel is examined as a function of the received OSNR and the study is subsequently extended to a seven-channel optical super-channel. The aim of the single-channel study is to optimise the parameters that do not depend on the crosstalk between channels. The optimal parameters obtained through simulation are listed in the *Design parameters* subsections at the end of sections 2.3, 2.4 and 2.5.

Next, in chapter 3, the various switching node configurations are evaluated. To do so, a route with a single node and variable transmission distances (both from transmitter to node and from node to receiver) is modelled. As was mentioned in section 1.2, the switching node is designed in the FOX-C project in a hierarchical way. At the fibre link level, two configurations have been considered in WP4 depending on the ultimate functionality of the specific node, but only the in-line ROADM node arrangement (Figure 3.1) has been analysed in the simulations carried out in T2.2 due to the nature of the route under examination. At the super-channel level, another two configurations have been investigated to handle the different flex-channel solutions generated by each of the five transceiver schemes proposed in chapter 0.

On the one hand, for the multi-band schemes based on AO-OFDM and N-WDM, an all-optical interferometric filter is described that ensures near-optimal matched filtering conditions for the clear extraction of a flex-channel from a super-channel and at the same time provides a novel phase regeneration stage for the addition of a new flex-channel to the aforementioned super-channel.

On the other hand, for the multi-band schemes based on electronic (F)OFDM and N-FDM, a high resolution filter allowing ultra-fine selectivity and adaptability to the spectral width of the non-overlapping flex-channels is described and its performance is investigated in terms of the received OSNR (both with and without transmission) for the case of a seven-channel optical super-channel in chapter 4.

Finally, in chapter 5 we present our conclusions.

1.4 Methodology

To analyse the performance of the different multiplexing schemes and the switching nodes, simulations are run in Matlab™. First, we define the time and frequency domain windows and then we generate random binary data and map them to OFDM subcarriers with 16QAM (28 sets of data are required for seven channels with 16QAM modulation). After the data are encoded, upsampling and filtering are used to emulate the effect of the arbitrary waveform generator, the sinc function during DAC, the pre-equalization, and the aliasing filter.

The modulation is based on the MZM transfer function and the laser phase noise and frequency instability are set to zero. At the receiver end, the signal is filtered by the OBPF, designed to have an ideal rectangular spectral profile with 2-GHz resolution. The signal is then detected and processed by a coherent receiver, where an additional 4th order Bessel electrical filter is used. A synchronization stage is not included in the simulation as these parameters can be known. Phase noise and frequency offset were not included either. The signal is finally equalized and decoded.

Before the OBPF we add ASE noise to evaluate the back-to-back performance of the different solutions. This way we can control the OSNR value and investigate the BER variation as a function of the OSNR. Table 1.1 shows a list of performance studies carried out for the three electrical multiplexing schemes under investigation in the FOX-C project along with references to the results obtained. Where it says "applicable", it means that the result obtained for the eOFDM case is applicable to the cases of eFOFDM and N-FDM.

Table 1.1 – List of back-to-back performance studies carried out for the electrical multiplexing schemes. All studies examined the cases of 20 and 40 zero-padded subcarriers, equivalent to 1-GHz and 2-GHz guard band between flex-channels, respectively.

BER vs.	eOFDM	eFOFDM	N-FDM
Single channel			
Input power into IQ modulator	Figure 2.12	*(applicable)*	*(applicable)*
Tx aliasing filter order	Figure 2.14	*(applicable)*	*(applicable)*
Rx OBPF bandwidth	Figure 2.15	*(applicable)*	*(applicable)*
Rx electrical filter bandwidth	Figure 2.16	*(applicable)*	*(applicable)*
FIR filter memory length	-	-	Figure 2.32
Rx OSNR (with optimised design parameters)	Figure 2.17, Figure 2.21	Figure 2.26	Figure 2.34
Seven-channel super-channel			
Tx aliasing filter order	Figure 2.18	*(applicable)*	*(applicable)*
Rx OBPF bandwidth	Figure 2.19	Figure 2.25	Figure 2.33
Rx electrical filter bandwidth	Figure 2.20	*(applicable)*	*(applicable)*
Rx OSNR (with optimised design parameters)	Figure 2.21	Figure 2.26	Figure 2.34

To model the switching node we assume that the transfer function of the filter is given by the convolution of the Gaussian filter (with a 1-, 1.5- and 2-GHz resolution) and a target filter. For the high spectral resolution (HSR) filter, the target filter is taken to be rectangular-shaped.

We also assume that the seven-channel super-channel generated at the transmitter travels along spans of SMF fibers of 80 km (with a total distance between 0 and 480 km), is then incident on a

network node with add/drop capabilities (where the 4th flex-channel is dropped), and subsequently the pass-through flex-channels, together with the added 4th flex-channel at the node, continue to travel along one or more spans of SMF fibers of 80 km (with a total distance between 0 and 480 km) to the receiver end. Transmission is based on the split-step Fourier method with the nonlinear coefficient set to zero and the step size set to 80 km to speed up the simulation (i.e. only dispersion and loss are included in the calculation. Because the system is considered linear, the step size can be very large).

At the end of each fiber (before the switching node and at the receiver), ASE noise is added to investigate the BER variation in terms of the OSNR. The performance of several flex-channels within the super-channel is evaluated, namely

- the BER of the 5th channel at the receiver
- the BER of the dropped 4th channel at the node drop port
- the BER of the added 4th channel at the receiver

Table 1.2 – List of performance studies carried out for the high spectral resolution (HSR) filter described in section 3.1.

<table>
<tr><th colspan="3">BER vs.</th><th>eOFDM</th><th>eFOFDM</th><th>N-FDM</th></tr>
<tr><td colspan="6">Transceiver + node design (without transmission)</td></tr>
<tr><td colspan="3">HSR filter bandwidth (for 1-GHz & 2-GHz guard band (GB) between flex-channels) [compare with Rx OBPF bandwidth in Table 1.1]</td><td>Figure 4.1</td><td>(applicable)</td><td>(applicable)</td></tr>
<tr><td colspan="3">Tx aliasing filter order (for 1-GHz/2-GHz GB)</td><td>Figure 4.2</td><td>(applicable)</td><td>(applicable)</td></tr>
<tr><td colspan="3">Rx electrical filter bandwidth (for 1-GHz/2-GHz GB)</td><td>Figure 4.3</td><td>(applicable)</td><td>(applicable)</td></tr>
<tr><td colspan="3">HSR filter bandwidth (for 2-GHz GB and 2-GHz, 1.5-GHz & 1-GHz filter resolution)</td><td>Figure 4.4</td><td>(applicable)</td><td>(applicable)</td></tr>
<tr><td colspan="3">Rx OSNR (with optimised design parameters, for 1-GHz/2-GHz GB and and 2-GHz, 1.5-GHz & 1-GHz filter resolution)</td><td>Figure 4.5</td><td>Figure 4.10</td><td>Figure 4.15</td></tr>
<tr><td colspan="6">Transmission effect (considering 1-GHz HSR filter resolution)</td></tr>
<tr><td rowspan="4">Fibre length before node when:</td><td colspan="2">Fibre length after node = 0;
guard interval (GI) length = 12 samples,
(for 1-GHz/2-GHz GB)</td><td>Figure 4.6</td><td>Figure 4.11</td><td>Figure 4.16
(GI length = 0)</td></tr>
<tr><td rowspan="3">Fibre length after node = 480 km</td><td>GI length = 12 samples (for 1-GHz/2-GHz GB)</td><td>Figure 4.7</td><td>Figure 4.12</td><td rowspan="3">Figure 4.17
(GI length = 0, 1-GHz/2-GHz GB)</td></tr>
<tr><td>GI length = 6 samples (for 2-GHz GB)</td><td>Figure 4.8</td><td>Figure 4.13</td></tr>
<tr><td>GI length = 0 (for 2-GHz GB)</td><td>Figure 4.9</td><td>Figure 4.14</td></tr>
</table>

Table 1.2 sums up the performance studies (both with and without transmission) carried out for the HSR filter and for the three electrical multiplexing schemes in T2.2 and shows references to the results obtained. Again, where it says “applicable”, it means that the result obtained for the eOFDM case is applicable to the cases of eFOFDM and N-FDM.

1.5 List of fixed parameters

A list of the fixed design parameters used in the simulations carried out in T2.2 can be seen in Table 1.3 below.

Table 1.3 – List of fixed transceiver, switching node and fibre parameters used throughout the document.

Transceiver parameters	
Modulation format	16QAM
Number of flex-channels in a super-channel	7
Rx OSNR	12.5 dB
Flex-channels whose performance is studied at final destination	Added 4th channel and 5th channel
Switching node parameters	
Number of nodes in the route	1
Dropped/added flex-channel	4th (middle channel)
Flex-channels whose performance is studied at network node drop ports	Dropped 4th channel
Fiber parameters	
Span length	80 km
Fibre type	SMF
Fibre loss	0.2 dB/km
Fibre dispersion	17 ps/nm/km
Maximum transmission distance	960 km (480 km before and after switching node)

2 Description of Transmitter-Receiver models and benchmarking results

This chapter sums up the transmitter-receiver implementations analysed in T3.2 and T3.3 and reported in D3.1, D3.2 and D3.3. It focuses on the design and parameters needed to carry out the simulations to investigate the performance of a **single optical channel** and a **seven-optical-channel super-channel** for each of the transceiver solutions.

In particular, two all-optical and three electronic implementations are being evaluated in the FOX-C project. Here we present the design characteristics and parameters of all of them and show the results of the performance investigation of the three electronic solutions.

For the electronic schemes, the performance is examined as a function of the received OSNR (for both one channel and a seven-channel super-channel) and also the bandwidth of the optical band-pass filter at the receiver (to filter out the desired optical channel from the super-channel). The optimal input power into the IQ modulator, the optimal order of the anti-aliasing super-Gaussian low-pass electrical filter at the transmitter and the optimal bandwidth of the 4th-order Bessel low-pass electrical filter at the receiver are also investigated.

2.1 Optical OFDM transceiver

In all-optical OFDM, the transmitter and receiver implementations are all optical and therefore any bandwidth limitations are due to the optical components and the RF circuits. These systems are based on well-established technologies, such as nested MZM, arrayed waveguide gratings (AWG), couplers, etc., and use a lower number of subcarriers, though with higher Baud rates than the electrical subcarriers in eOFDM. AO-OFDM implementations are of great importance as they combine the spectral efficiency advantages of OFDM multiplexing without guard band to generate high capacity volumes.

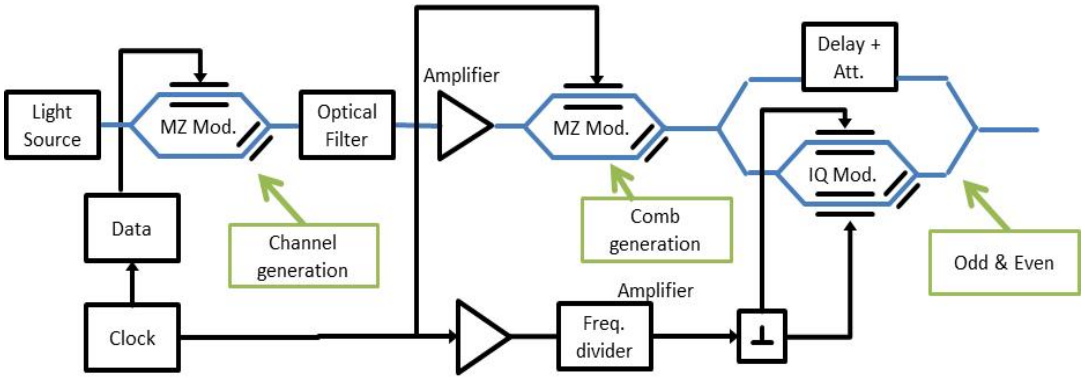

Figure 2.1 – AO-OFDM transmitter schematic

2.1.1 Optical OFDM transmitter model and set-up

Figure 2.1 shows the AO-OFDM transmitter schematic (for an experiment conducted in WP3). A narrow line-width fibre laser creates a 16 dBm cw signal, which is subsequently modulated at a bit rate of 20 Gbit/s. The 20-GHz clock is doubled and used to drive a MZM to replicate the modulated signals to five copies with 40-GHz channel spacing. Subsequently the channels are launched to an optical interferometer for creating the odd and even channels. In the upper arm, there is an optical delay line, which introduces a delay equivalent to an integer number of bits, and a variable attenuator for power equalization. In the lower arm, there is a frequency shifter based on a Dual-Parallel Mach-Zehnder Modulator (DP-MZM) driven by both cosine and sine waveforms centred at 20 GHz. A phase shifter in one of the two RF paths ensured control of the relative phase differences between the two driving

signals. The RF signal has been taken from the same clock that drives the pattern generator. The odd and even channels are equally spaced by a difference equal to the sub-channel's bit rate (i.e. 20 GHz). The two paths are combined to form the all-optical OFDM super-channel.

2.1.2 Optical OFDM receiver model and set-up

For receiving the all-optical FOFDM signal, demultiplexing of its sub-channels is required. In the last section, the demultiplexing of eFOFDM is facilitated digitally, through the implementation of the discrete cosine transform in the electrical domain. However, to be able to handle high- bandwidth all-optical FOFDM super-channels, a corresponding demultiplexing scheme needs to be developed in the optical domain. Such a scheme is depicted in Figure 2.2. It comprises an all-optical FFT processor and a black-box phase-sensitive amplifier (PSA), which enables full suppression of the interchannel crosstalk. At the input stage of the amplifier, the signal is combined with a local pump (pump 1) and it is subsequently mixed in a nonlinear medium (e.g. a HNLF). Modulation stripping is thus achieved and a carrier is extracted symmetrically to the signal. After the nonlinear element (NE), a coupler splits the optical signals in two arms. In the lower arm, a filter selects the extracted carrier and a subsequent SSB modulator introduces an additional frequency shift to the wave equal to half of the bitrate. The modulator is driven by a clock signal extracted from the OFDM super-channel. The frequency-shifted carrier then phase-locks a local laser oscillator to create a second synchronized pump for the PSA (pump 2). Next, a multiplexer (e.g. a WSS unit) combines pump 2 along with pump 1 and the selected sub-channel –the one that propagates in the upper arm— and directs them to a second nonlinear medium, where a phase sensitive four-wave mixing process takes place.

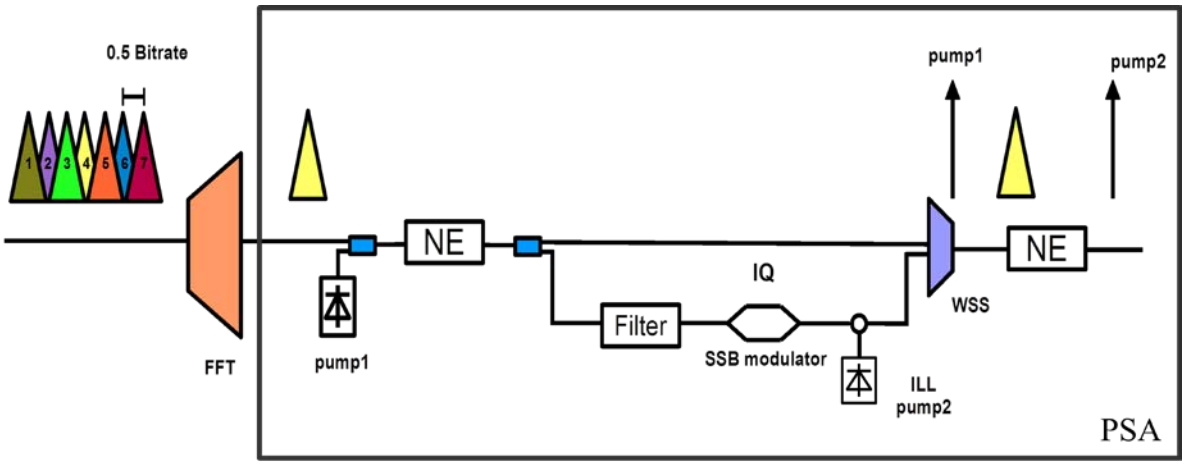

Figure 2.2 – AO-OFDM receiver processing schematic: FFT + Phase Sentitive Amplifier (PSA)

2.1.3 Design remarks and parameters

Table 2.1 – AO-OFDM design parameters.

PPG	Maximum Baud Rate	12.5 GBd
	PRBS range	2^{31}
Data modulator	Bandwidth	40 GHz
	Single Drive	-
Comb generator modulator	Bandwidth	40 GHz

	Single Drive	-
Frequency shifter modulator	Bandwidth	20 GHz
	Extinction Ratio	>30 dB
	IQ Modulator	-
Laser	Wavelength	1552.3 nm
	Linewidth	< 1 kHz
Photodetector	Bandwidth	32 GHz
All-optical FFT processor		
Phase sensitive amplifier (PSA)	Nonlinear Element (HNLF) (x2)	
	SSB modulator	
	Laser pump (x2)	
	Multiplexer (e.g. WSS)	

2.2 Nyquist WDM transceiver

In the Nyquist WDM approach each sub-channel spectrum is rectangular-shaped in the optical domain. The super-channel comprises several rectangular-shaped sub-channels which do not overlap and are independent, thus making phase control of the different carriers unnecessary. However, optical filters with a high resolution and sharp edges are needed to achieve the best possible transmission quality. Similarly, the generation of signals with rectangular-shaped spectrum requires DSP hardware with highest performance.

2.2.1 NWDM transmitter model and set-up

ASTON will investigate two implementations of a NWDM transmitter unit. The first will be based on the use of an all-optical filter with rectangular transfer function for performing the Nyquist pulse reshaping. The second approach will enable the pulse reshaping in the electrical domain based on suitable analogue electrical filters. In the experimental implementation of the schemes the same diagram of Figure 2.1 will be used with minor modifications. For the first case the optical filter located after the data modulator (see Figure 2.1) will play the pulse reformatting role. The optical filter will not be required in the second implementation since we will use electrical FIR filters. The comb generation part of the transmitter will remain the same for both cases as described in the figure.

The aforementioned transmitter architecture is suitable only for the purposes of an experimental demonstration and it allows only the generation of de-correlated odd-even sub-channels. In simulations we can consider a more generalized architecture for super-channel creation. For the two approaches described above the simulation models are depicted in Fig. 2.3 a) and b).

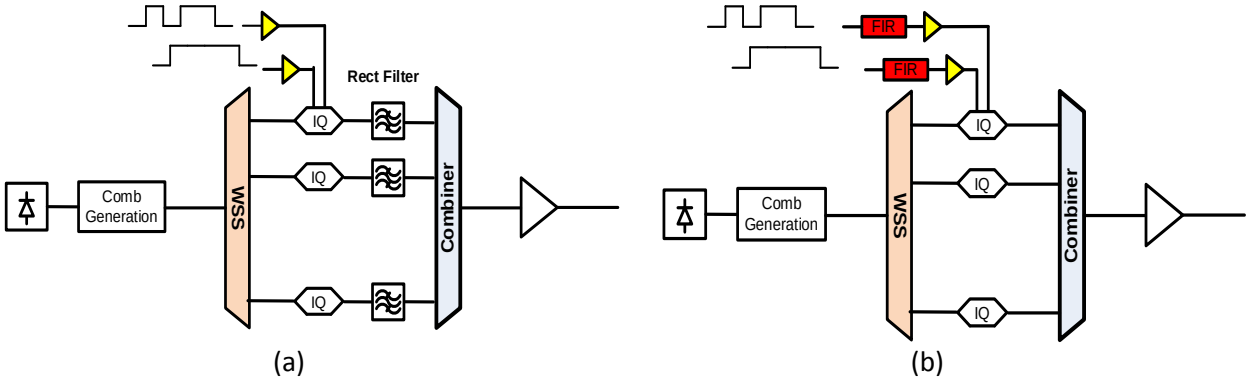

Figure 2.3 – (a) Modelling diagram of Nyquist WDM transmitter which achieves pulse reshaping with the use of filters with rectangular transfer function. (b) Alternative implementation of the Nyquist WDM transmitter based on electrical FIR filters.

Figure 2.3(a) shows the setup of a NWDM super-channel transmitter with optical pulse reshaping. A CW laser light is fed into a comb generator which creates the multiple optical carriers of equal intensity and constant phase difference located at a fixed channel spacing that equals the modulation baud-rate. Uncorrelated pulse-streams are encoded by an array of IQ modulators in the optical domain. At the output of each modulator a rectangular filter will reshape each pulse-stream and subsequently the sub-channels will be combined to form the super-channel. For the second case shown in Figure 2.3(b), electrical FIR filters are placed at the driving electronics of each modulator, making the optical filters unnecessary, so they are omitted from the model setup.

2.2.2 NWDM receiver model and set-up

To demultiplex a Nyquist WDM super-channel match filtering will be required at the receiver. Again here there are two options, to use rectangular filtering either in the optical domain or in the electrical domain. Regarding the receiver architecture, coherent detection has been considered. The two variations are illustrated in Figure 2.4(a) and (b).

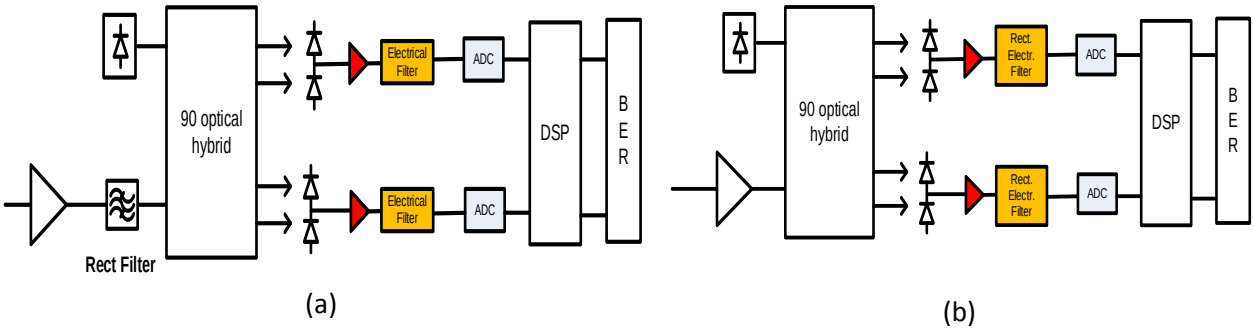

Figure 2.4 – Modelling diagram of coherent receiver for the detection of Nyquist sub-channels (a) using optical match filter at the receiver, and (b) using electrical matched filter.

2.2.3 Design parameters

Transmitter parameters	Optical channel number	7
	Modulation format	BPSK up to 16 QAM
	Channel spacing	12.5 GHz
	Spectral profile of the Nyquist	10th-order Gaussian

	filter	
	Bandwidth	12.5 GHz
	Linewidth	<10 kHz
Receiver parameters	Frequency offset between the transmitter laser and local oscillator	0 MHz
	Photodiode responsivity	0.6 A/W
	Thermal noise power density	100 pA/Hz1/2
	Electrical filter bandwidth	12.5 GHz
PPG	Maximum Baud Rate	12.5 GBd
	PRBS range	2^{31}
BER estimation	Monte Carlo	Less than 10% variation
	Noise figure of optical amplifiers	5 dB

2.3 Electronic OFDM (eOFDM) transceiver

This section describes the design of the flexible eOFDM transceiver. It starts with the description of the transmitter and receiver designs, and concludes with the results of the simulation and a list of the parameters used.

2.3.1 eOFDM transmitter model and design remarks

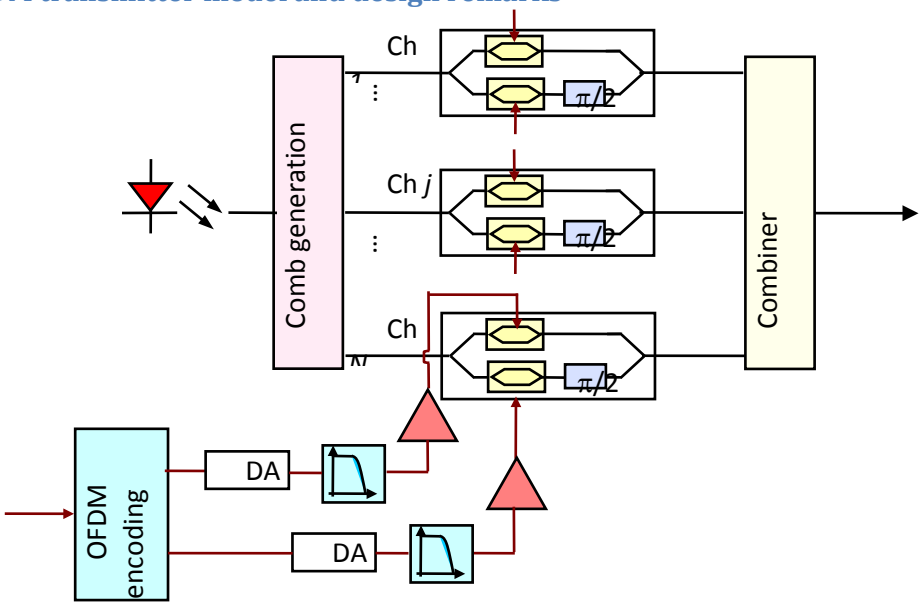

Figure 2.5 – Setup of eOFDM-based optical super-channel transmitter

Figure 2.5 – shows the setup of eOFDM-based optical super-channel transmitter. A continuous wave (CW) light from a laser is fed into an optical comb generator to obtain multiple optical carriers with equal intensities and phases. The channel spacing is 12.5 GHz. Uncorrelated eOFDM signals are encoded using the DSP procedures as illustrated in .

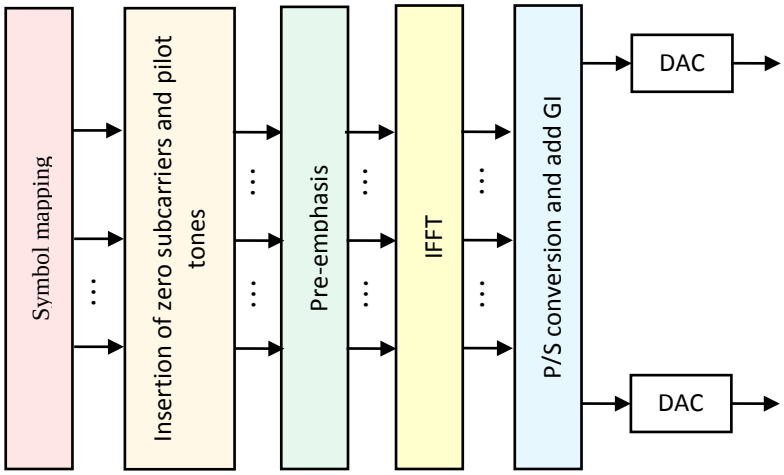

Figure 2.6 – DSP for OFDM signal encoding

The inverse fast Fourier transform (IFFT) is used to multiplex the subcarriers with *N* points, where *N* is equal to 256 throughout the simulations in this report. Four subcarriers in the zero-frequency region are not modulated allowing for AC-couple amplifiers and receivers. 16QAM formats are used on eOFDM data modulation subcarriers, and the subcarriers in the high-frequency region are zero-padded to avoid aliasing. The number of zero-padded subcarriers is adjusted to investigate the performance of back-to-back transceivers and that with channel add/drop in the network nodes. The mapped signal is pre-emphasized to equalize the sinc-function roll-off during digital-to-analogue conversion and the analogue bandwidth of the digital-to-analogue converter (DAC). After IFFT and parallel-to-serial (P/S) conversion, samples are added to each symbol as a guard interval (GI) and then the serial signal is clipped to control the peak to average power ratio. The eOFDM signals are converted to analogue signals using 12.5-GS/s digital-to-analogue converters. Low-pass electrical filters are applied to filter out the aliasing. The bandwidth and spectral response of the filters are controlled to investigate the transceiver performance. The signals are amplified by electronic drivers and modulated onto each optical carrier. The input electrical signal level into the modulators is varied to investigate the nonlinear effect during modulation.

Several design issues are addressed. At the transmitter, high-frequency subcarriers are zero-padded to avoid the aliasing effect [1] and pre-emphasis is used to equalize the sinc-function rolloff in DAC. Assuming s_n is the n^{th} time-domain sample, the generated analogue signal from DAC can be represented as the convolution of s_n and a rectangular function with the pulse width of the T/N. In the frequency domain, it corresponds to the multiplication of the signal spectrum with a sinc function. Figure 2.7 shows the sketched discrete signal before DAC and the converted analogue signal after DAC. Figure 2.8 shows the signal spectrum evolution during this process. It can be seen that the main lobe is distorted by multiplying the sinc-function with higher attenuation at higher frequencies. The aim of pre-emphasis is to pre-equalize this effect and the associated analogue bandwidth in DAC such that the signal after DAC has no spectral distortion. In addition, it can be seen from Figure 2.8 that there are side lobes in the spectrum (aliasing). In practice, a low-pass filter is required to filter out the aliasing. Due the fabrication difficulty of electrical filter with sharp rolloff, a guard band between the main lobe and the aliasing is required. This is realized by setting high-frequency subcarriers un-modulated as described above.

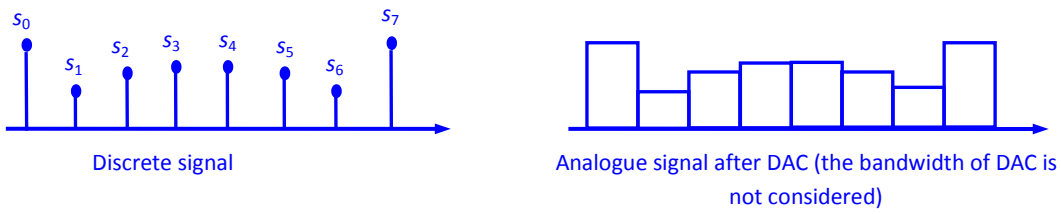

Figure 2.7 – Sketched discrete signal before DAC and converted analogue signal after DAC

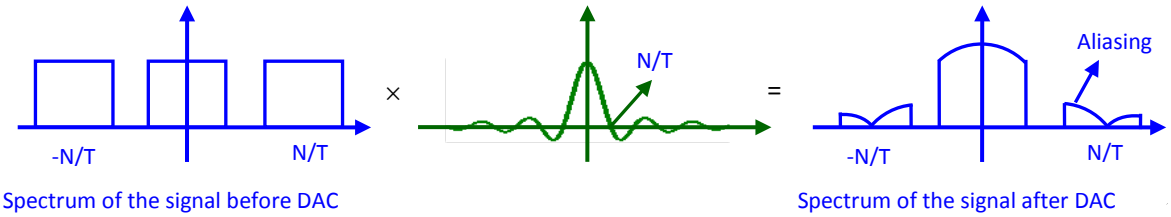

Figure 2.8 – Spectrum evolution through the DAC

In conventional OFDM, in order to enable dispersion compensation using simple one-tap equalizer after FFT, cyclic prefix based guard interval is used to avoid the ICI and ISI [1-4]. Figure 2.9 illustrates an example of the cyclic-extension based guard interval in OFDM.

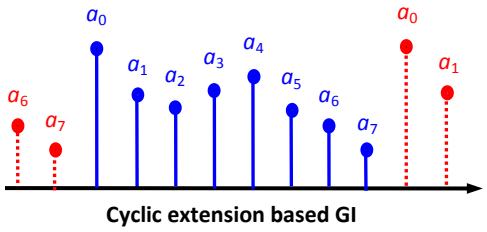

Figure 2.9 – Guard interval design in OFDM

The generated time-domain OFDM signal has high peak to average power ratio due to a large number of subcarriers. Therefore, the power into the I/Q modulator should be controlled. A balance between signal nonlinear distortion and output signal power is needed and there is an optimal electrical input power. This issue will be investigated in the following simulations.

2.3.2 eOFDM receiver model and design remarks

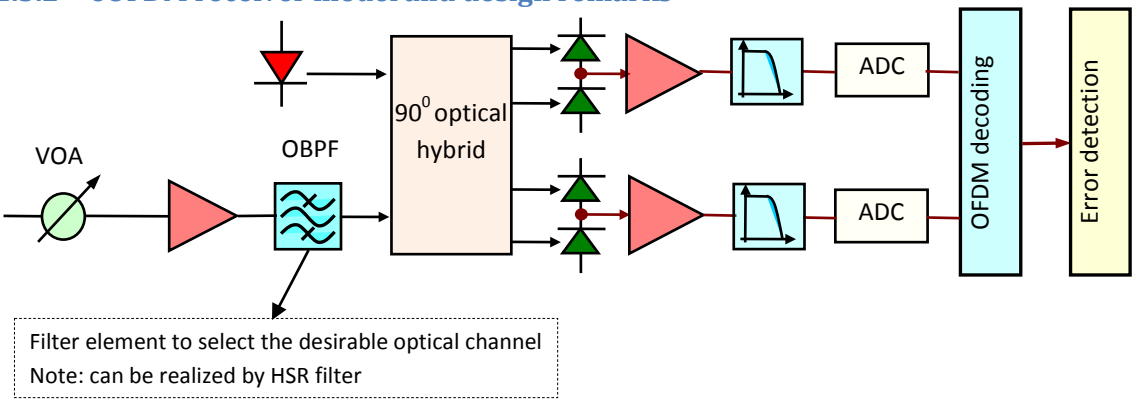

Figure 2.10 – Model of eOFDM receiver

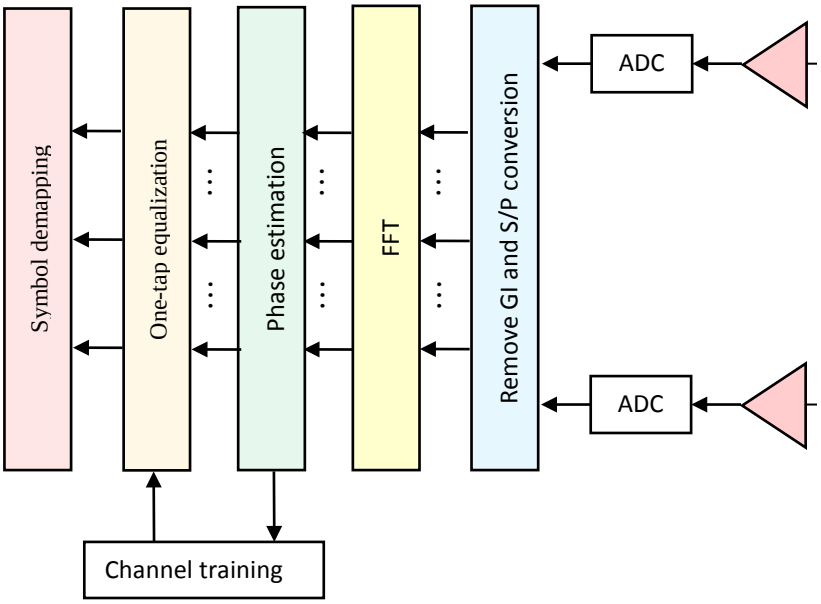

Figure 2.11 – DSP procedure for eOFDM decoding

Figure 2.10 shows the model of the eOFDM receiver while the DSP procedure for eOFDM decoding is illustrated in Figure 2.11. At the receiver, the signal power into the preamplifier is adjusted to control the OSNR. An optical band-pass filter is used to filter out the desired optical channel. The functionality of this filter can be realized by high spectral resolution filter in the network configuration. The bandwidth and the resolution of this filter are essential to optimize the performance of not only the dropped channel but also the other through channels. When the bandwidth is wide, the filter can pass through the whole desirable channel but with additional power from adjacent channels. The adjacent channels through the node would be degraded due to the power loss filtered by the filter. On the other hand, when the bandwidth is narrow, the drop channel is distorted while the signals passing through this node would have residual power of the dropped channel. The network configuration will be investigated in detail in section 4. In this section, we only consider the performance of the desired channel (i.e. without considering the performance of other channels). Coherent detection is used after demultiplexing [5]. The signal and local oscillator are mixed by a 90^0 optical hybrid, and detected by balanced detectors to extract the in-phase and quadrature components. The powers of the local oscillator and the received signal are 10 dBm and 0 dBm respectively, and their polarizations are controlled to be the same. The equivalent thermal noise spectral power density of the detectors is $100pA/Hz^{1/2}$ and the responsivity of photodiodes is 0.6 A/W. After detection, the signals are electrically amplified and filtered by 4^{th}-order Bessel electrical filters. The bandwidth of the filters is varied for investigation. The received analogue signals are sampled by ADCs and decoded using DSP algorithms. Each FOFDM symbol is serial-to-parallel converted and FFT is applied to transform the time-domain signal to the frequency domain. By using cyclic extension based guard interval, dispersion can be compensated using one-tap equalizers. On the other hand, the coefficients of the one-tap equalizers should be estimated, which is achieved by using training symbols (TSs) [6]. Time-domain averaging algorithm that averages over multiple TSs is used in this report to mitigate the noise effect. After channel equalization, the symbols are de-mapped and bit error rate is calculated using direct error counting.

2.3.3 Performance investigation

In this section, we will firstly investigate the performance of single optical channel and then extend the study to a seven-channel optical super-channel. The aim of the single-channel study is to optimize some parameters that do not depend on the crosstalk between channels and also to provide the comparison line for the optical super-channel case.

We set the number of zero-padded subcarriers to be 20 and 40, corresponding to around 1 GHz and 2 GHz in the spectrum under 256 total subcarriers and 12.5-GS/s DAC. The aliasing filter is assumed to

exhibit a super-Gaussian spectral profile and the OBPF at the receiver is the high spectral resolution filter whose transfer function is defined in section 3.

Firstly, we study the input power into the IQ modulator to avoid the nonlinear effects while maximizing the output after modulation. Figure 2.12 shows the BER versus the normalized average power into the modulator. The power is the total power from both the I and Q arms. The number of zero-padded subcarriers is 20 (triangles) and 40 (circles). The OSNR is 12.5 dB. The bandwidth of the OBPF is 12 GHz and an 8th-order Gaussian-shaped filter is used to filter out the aliasing. At the receiver, the electrical filter bandwidth is 4 GHz. It can be seen that the performance improves as the power reduces and at -11 dBm, the performance can realize an optimal value. It is also seen that the performance using 40 zero-padded subcarriers is better than that using 20 zero-padded subcarriers even under sufficiently small electrical power. In the single-carrier case, this improvement is due to the reduced data rate. In the multiple channel case that is investigated later, the control of the number of zero-padded subcarriers would adjust the guard band between channels and has different requirement on the specifications of the OBPF and the aliasing filter. In the following simulations, we will fix the normalized input power to be -12 dBm to avoid the nonlinear effects in the modulator.

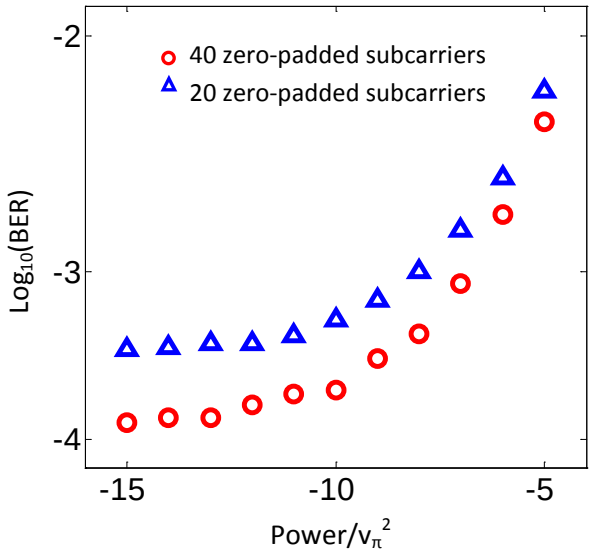

Figure 2.12 – Performance versus the normalized power into the modulator

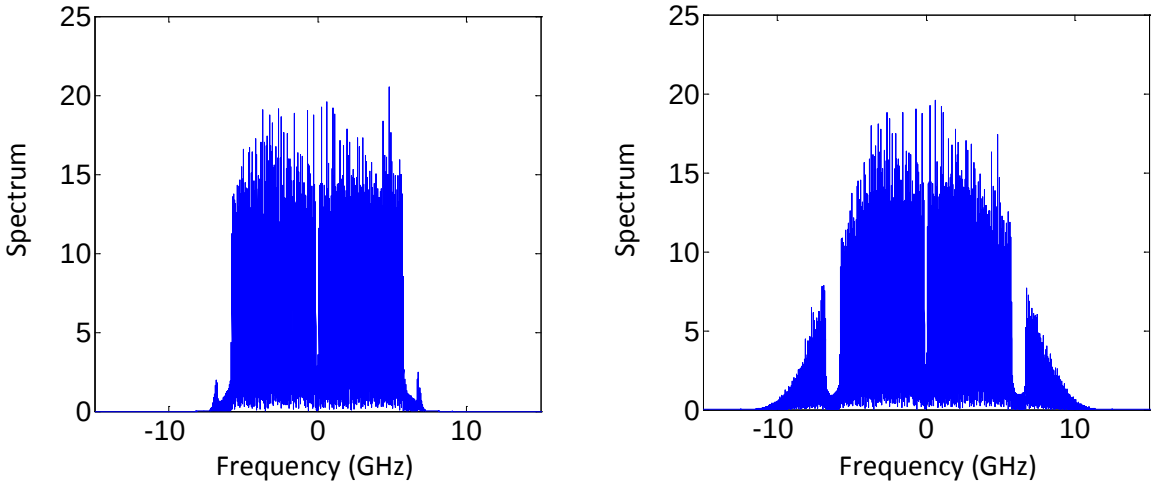

Figure 2.13 – Spectrum after the aliasing filter when 8th-order and 2nd-order Gaussian filter is used. The number of zero-padded subcarriers is 20.

One of key issues in the design is the aliasing filter which filters out the adjacent side lobes in Figure 2.8. Figure 2.13 shows the electrical spectrum after the aliasing filter when the filter has the spectral profile of 8th-order (left) and 2nd-order (right) Gaussian. It can be seen that an 8th-order Gaussian filter has a sharp rolloff so can filter out almost all aliasing without significant distortion on the main lobe. When 2nd-order Gaussian filter is used, residual aliasing exhibits. Note that the residual aliasing may not degrade the performance severely in the single-channel case. It only introduces extra power loss to the system without any crosstalk effects. Figure 2.14 shows the performance at 12.5-dB OSNR when the OBPF bandwidth is 12 GHz and the electrical filter bandwidth at the receiver is 4 GHz. It is confirmed that the performance is not very sensitive to the aliasing filter spectral profile for both 20 and 40 zero-padded subcarriers in the single-channel case provided that the order number is larger than 3. The BER variation is less than one order of magnitude when the order number changes from 1 to 10. It is also seen that the performance is near optimal when the order number is larger than 4 in the single-channel case. Note that in the optical super-channels cases, residual aliasing would corrupt adjacent channels and much more careful aliasing filter design is required. The results in Figure 2.14 can be used as a reference to compare with the super-channel case.

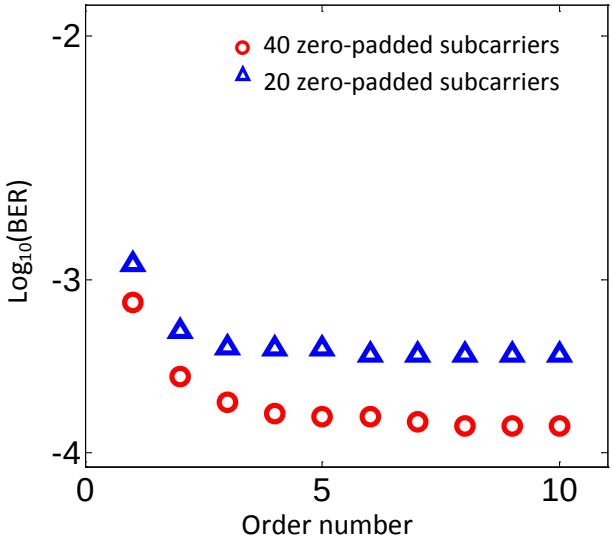

Figure 2.14 – Performance versus the order number of the Gaussian aliasing filter. The filter bandwidth is 6.25 GHz.

Figure 2.15 shows the performance versus the bandwidth of the OBPF at the receiver. The OBPF is designed to have an ideal rectangular spectral profile with 2-GHz practical resolution. Detailed filter spectral profiles can be found in Section 3. When the filter bandwidth is narrow, the signal is distorted due to intersymbol interference. When the filter bandwidth is wide, more optical noise would pass through the filter and degrade the performance. The optimal value depends on the balance between these two effects and is around 10-12 GHz. It can also be observed that in the single-channel case, the performance is not very sensitive to the OBPF bandwidth.

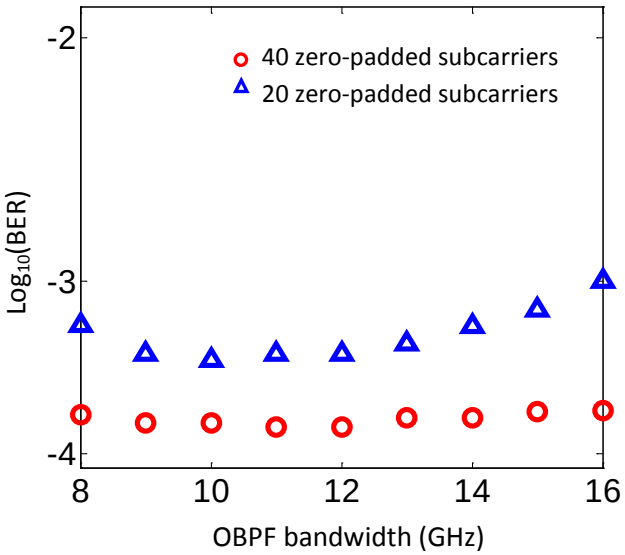

Figure 2.15 – Performance versus the OBPF bandwidth with 2-GHz filter resolution

Figure 2.16 depicts the performance versus the bandwidth of the electrical 4th-order Bessel filter at the receiver. The optical filter bandwidth is 12 GHz. In coherent detection with single channel, the functionality of the electrical filter under optimized OBPF bandwidth is mainly to filter out the photodiode thermal noise. In the optical noise limited operation region, the received power is sufficiently high and the thermal noise effect is negligible. Therefore, under a fixed and optimal OBPF bandwidth, the performance does not vary with electrical filter bandwidth in the single channel case unless the filter bandwidth is too narrow to introduce distortion to the signal.

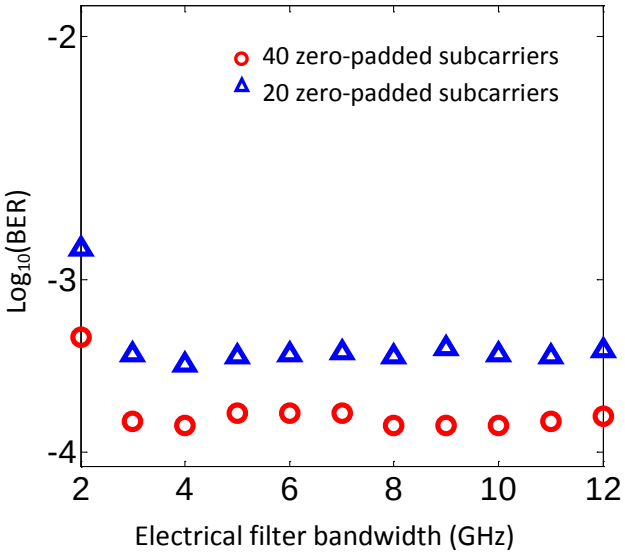

Figure 2.16 – Performance versus the bandwidth of the electrical filter at the receiver

Finally, we depict the BER performance versus the received OSNR under optimized system parameters as illustrated above and the result is shown in Figure 2.17. The performance difference between 40 and 20 zero-padded subcarriers is mainly from the fact that the data rates are not the same.

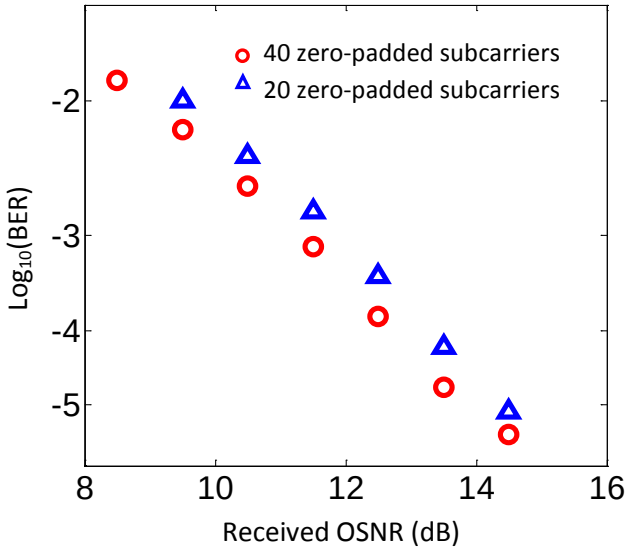

Figure 2.17 – Performance versus received OSNR under optimized system parameters

Next, we will extend the investigation to seven channels. The channel spacing is 12.5 GHz and the data encoded on to different channels are uncorrelated. In each channel, we fix the normalized input power to the modulator as -12 dBm and will particularly show that the specification requirements of the OBPF and the aliasing filter are significantly enhanced when compared to the single-channel case. Figure 2.18 shows the BER versus the order number of the aliasing filter when 20 and 40 subcarriers at the high-frequency region are zero-padded. These correspond to 1 and 2-GHz guard band between adjacent channels. The bandwidths of the OBPF and electrical filter at the receiver are optimized. We can see that when compared to Figure 2.14, the performance is more sensitive to the order number in the super-channel case. It is because any residual aliasing would introduce crosstalk to adjacent channels so should be removed perfectly. When 40 subcarriers are used, the guard band between channels is large (2 GHz) so the requirement on the order number is not as strict as that for 20 zero-padded subcarriers (1 GHz). The performance begins to saturate when the order number is larger than 6. On the other hand, when 20 zero-padded subcarriers are used, filter with sharper edges should be used to obtain the optimal performance and we can see that the system is not optimal yet even when the order number increases to 10. In practice, due to the fabrication difficulty, we assume 8^{th}-order Gaussian aliasing filter unless otherwise stated.

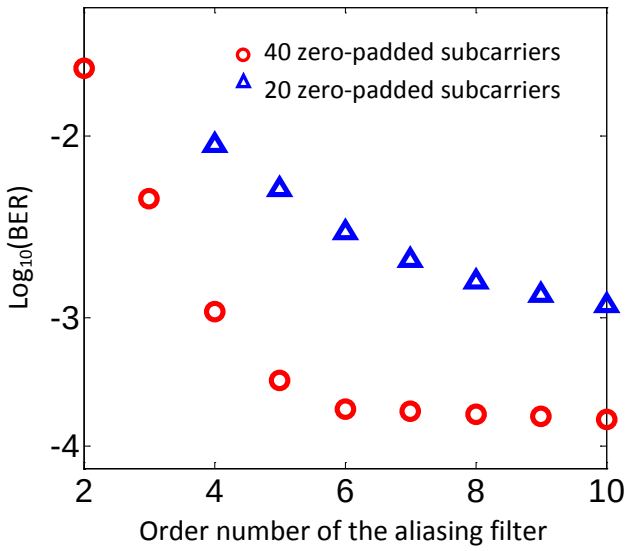

Figure 2.18 – Performance versus the order number of the Gaussian aliasing filter for 1-GHz and 2-GHz guard band. The filter bandwidth is 6.25 GHz.

Figure 2.19 shows the BER versus the bandwidth of the OBPF for channel demultiplexing. As expected, the performance sensitivity to the filter bandwidth is higher compared to Figure 2.15. In both cases of the figure, the optimal bandwidth is around 10 GHz. It can also be seen that under optimized bandwidth, the performance using 2-GHz guard band exhibits negligible penalty when compared to the single channel case, with the best BER around 1.7×10^{-4} at 12.5-dB OSNR. In contrast, when 1-GHz guard band (or 20 zero-padded subcarriers) is used, the optimal performance when compared to the single-channel case is significantly degraded due to the residual crosstalk from adjacent channels.

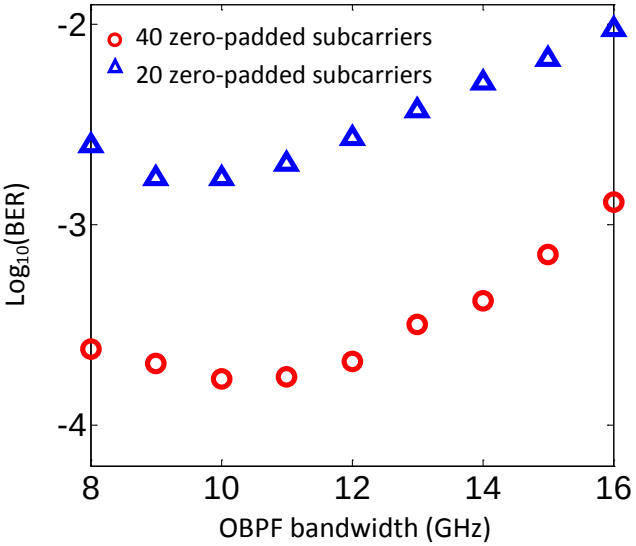

Figure 2.19 – Performance versus the bandwidth of the OBPF

The performance sensitivity to the bandwidth of the electrical filter is also increased slightly, as illustrated in Figure 2.20. It is because although the crosstalk and intersymbol interference have been balanced by the OBPF, residual crosstalk after the OBPF still exists. When the electrical filter bandwidth is narrow, the crosstalk can be further suppressed unless the signal is highly distorted due to the intersymbol interference (the case when the electrical filter bandwidth is 2 GHz). The optimal filter bandwidth is around 3 GHz that is used for the following investigations unless otherwise stated.

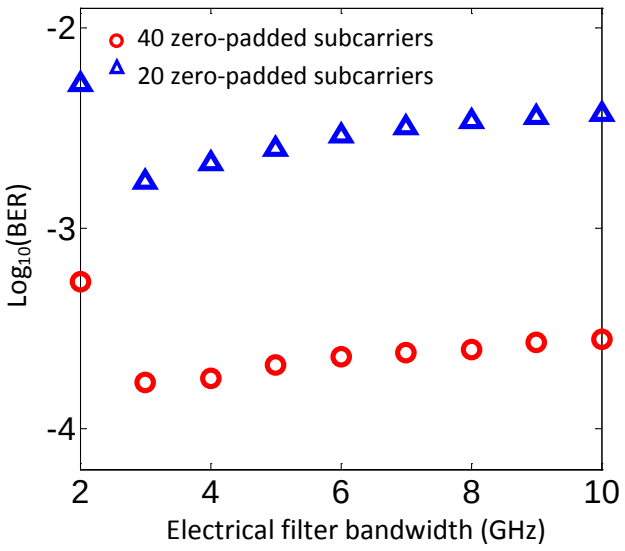

Figure 2.20 – Performance versus the bandwidth of the electrical filter at the receiver

Finally, the BER versus the received OSNR when the system parameters are optimized is illustrated in Figure 2.21. In the figure, we have also provided the curves of the single-channel case. It can be seen that when 2-GHz guard band is used, the performance is very similar to the single channel case, implying negligible penalty arising from the crosstalk from adjacent channels. However, when 1-GHz guard band is used, the performance is significantly degraded and error floor is observed. Note that the optical filter in the results is a high spectral resolution filter with 2-GHz resolution.

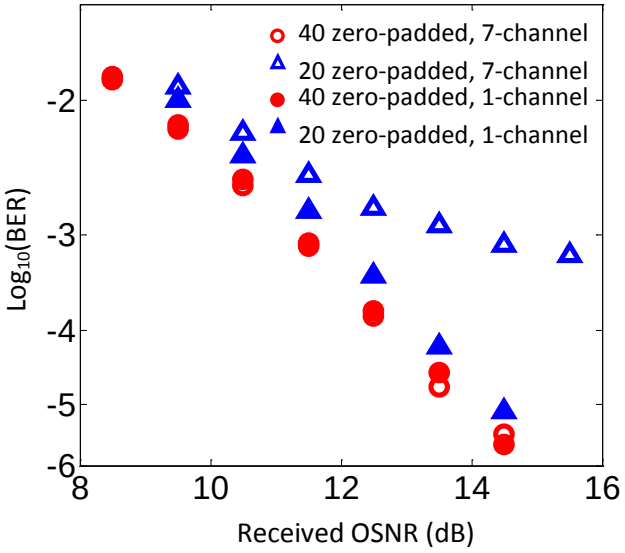

Figure 2.21 – Performance versus the received OSNR for single and seven channel cases

2.3.4 Design remarks and parameters

Table 2.2 – eOFDM design parameters.

Transmitter parameters	Optical channel number	7
	Modulation format	16QAM
	Total OFDM subcarrier number	256
	Zero-padded subcarrier number	20/40
	DAC sampling rate	12.5 GS/s
	Channel spacing	12.5 GHz
	Bandwidth of the aliasing filter	6.25 GHz
	Spectral profile of the aliasing filter	8^{th}-order Gaussian [optimal: ≥4 for single channel studies; ≥6 and >10 for 7-channel-superchannel with 40 and 20 zero-padded subcarriers, respectively]
	Normalized power into the modulator	-12 dB (optimal)
	Guard interval type	Cyclic extension
	Length of guard interval	12 samples

Receiver parameters	Frequency offset between the transmitter laser and local oscillator	0 MHz
	Photodiode responsivity	0.6 A/W
	Thermal noise power density	100 pA/Hz$^{1/2}$
	Electrical filter bandwidth	3 GHz (optimal) [4 GHz used for single-channel studies. For single-channel channel, optimal value ≥3 GHz. For 7-channel-superchannel, optimal value 3 GHz]
	Electrical filter profile	4th-order Bessel
	OBPF bandwidth	12 GHz [optimal: 10-12 GHz for single channel studies; 10 GHz for 7-channel-superchannel]
	OBPF resolution	2 GHz

2.4 Electronic fast-OFDM (eFOFDM) transceiver

This section describes the design of the flexible eFOFDM transceiver. It starts with the description of the transmitter and receiver designs, and concludes with the results of the simulation and a list of the parameters used.

2.4.1 eFOFDM transmitter model and set-up

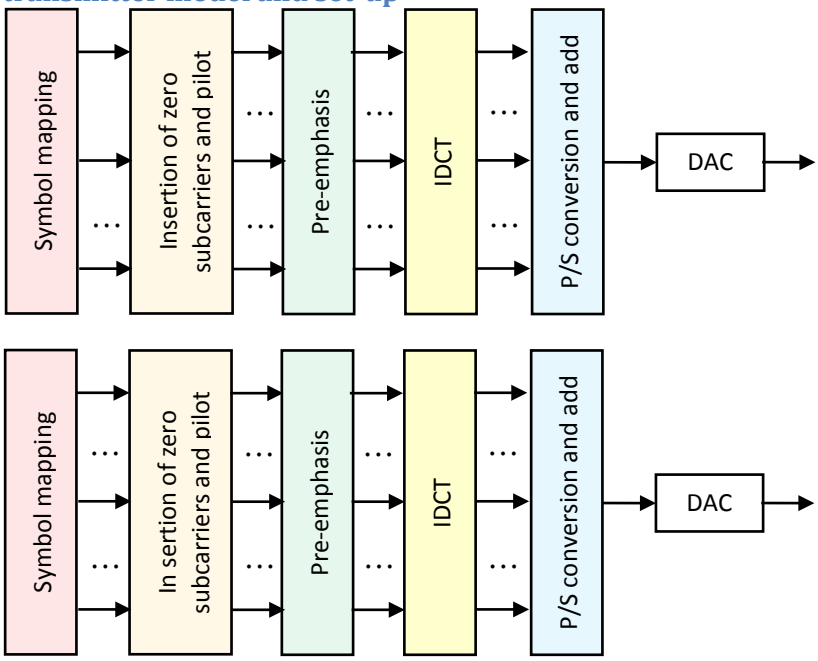

Figure 2.22 – DSP procedure of electrical fast OFDM

The transmitter setup of electrical fast OFDM is similar to the conventional OFDM except that different DSP procedure [7-9] should be applied for fast OFDM signal encoding. Figure 2.22 illustrates the DSP procedure. The inverse fast discrete cosine transform (IDCT) is used to multiplex the subcarriers with *N* points, where *N* is equal to 256. 16QAM formats are used on eFOFDM data modulation subcarriers, and the subcarriers in the high-frequency region are zero-padded to avoid aliasing. The number of zero-padded subcarriers is either 20 or 40, corresponding to 1 GHz or 2 GHz guard band between channels. The mapped signal is pre-emphasized to equalize the sinc-function roll-off during digital-to-analogue conversion and the analogue bandwidth of the digital-to-analogue converter (DAC). After IDCT and parallel-to-serial (P/S) conversion, samples are added to each symbol as a guard interval (GI). Different from conventional OFDM, symmetric extension rather than cyclic extension based GI is used to enable single-tap equalization at the receiver [10]. Figure 2.23 shows an example of symmetric extension based GI, where *N* is assumed to be 8. The eFOFDM signals are converted to analogue signals using 12.5-GS/s digital-to-analogue converters. Low-pass electrical filters are applied to filter out the aliasing. The bandwidth of the filter is 6.25 GHz and the spectral profile is 8^{th}-order Gaussian. The signals are amplified by electronic drivers and modulated onto each optical carrier. The input electrical signal power into the modulators is -12 dB with respect to V_π^2. In the optical domain, seven channels are used with channel spacing of 12.5 GHz.

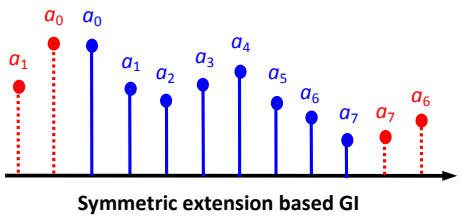

Figure 2.23 – Symmetric extension based GI for dispersion compensation in eFOFDM.

2.4.2 eFOFDM receiver model and set-up

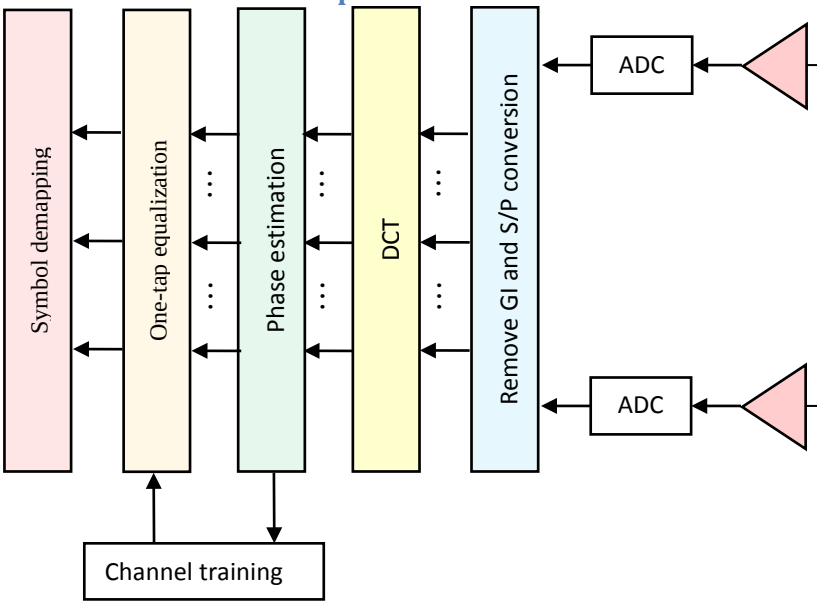

Figure 2.24 – DSP procedure at the receiver for eFOFDM decoding

The receiver setup is the same as Figure 2.10 while the DSP procedure for eFOFDM is illustrated in Figure 2.24. The powers of the local oscillator and the received signal are 10 dBm and 0 dBm respectively, and their polarizations are controlled to be the same. The equivalent thermal noise spectral power density of the detectors is 100pA/Hz$^{1/2}$ and the responsivity of photodiodes is 0.6 A/W. After detection, the signals are electrically amplified and filtered by 4th-order Bessel electrical filters with 3-GHz bandwidth. The received analogue signals are sampled by ADCs and decoded using DSP algorithms. Each FOFDM symbol is serial-to-parallel converted and DCT is applied to transform the time-domain signal to the frequency domain. By using symmetric extension based guard interval, dispersion can be compensated using one-tap equalizers. On the other hand, the coefficients of the one-tap equalizers are estimated based on the time-domain averaging algorithm. After channel equalization, the symbols are de-mapped and bit error rate is calculated using direct error counting.

2.4.3 Performance results

In this subsection, we will study a seven-channel eFOFDM super-channel. Additional results show that the parameters such as input power into the modulator, electrical filter bandwidth, etc. are similar to those of conventional OFDM. Figure 2.25 depicts the performance versus the OBPF filter bandwidth for the eFOFDM super-channel. The OSNR is 12.5 dB. It can be seen that the optimal bandwidth is 8-10 GHz and when increasing the filter bandwidth, power from adjacent channels would be filtered into the desirable channel and degrade the performance. By comparing Figure 2.25 and Figure 2.19, we can see that the performance of conventional eOFDM and eFOFDM at the optimal OBPF bandwidth is similar.

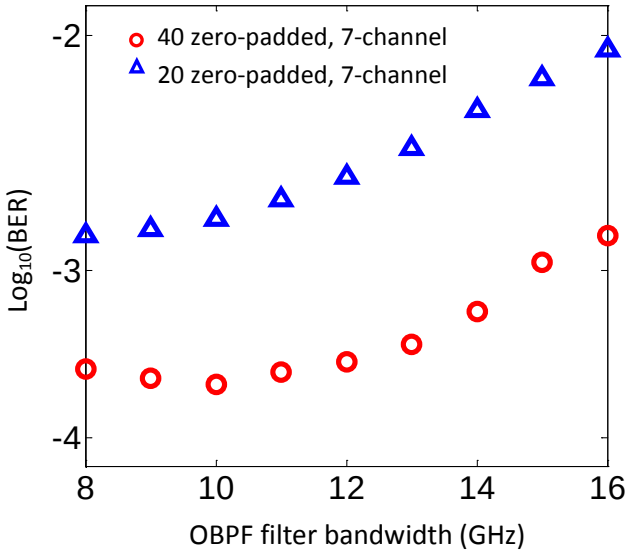

Figure 2.25 – Performance versus the bandwidth of the OBPF

Figure 2.26 shows BER versus the received OSNR for single-channel and seven-channel systems when 40 or 20 subcarriers are zero-padded. It can be seen that under the optimized system performance and using 40 zero-padded subcarriers (2-GHz guard band), the super-channel performance is very similar to the single-channel case. On the other hand, when the guard band decreases to 1 GHz, crosstalk between channels exists and error floor is observed.

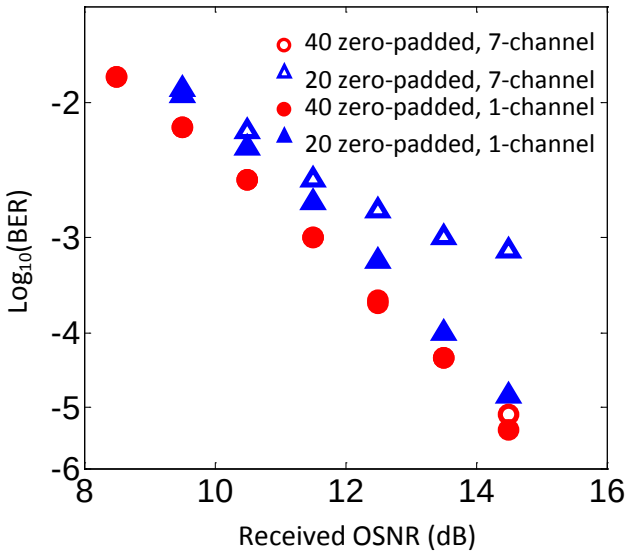

Figure 2.26 – Performance versus the received OSNR for single and seven channel cases

2.4.4 Design parameters

Table 2.3 – eFOFDM design parameters.

Transmitter parameters	Optical channel number	7
	Modulation format	16QAM
	Total FOFDM subcarrier number	256
	Zero-padded subcarrier number	20/40
	DAC sampling rate	12.5 GS/s
	Channel spacing	12.5 GHz
	Bandwidth of the aliasing filter	6.25 GHz
	Spectral profile of the aliasing filter	8^{th}-order Gaussian
	Normalized power into the modulator	-12 dB
	Guard interval type	Symmetric extension
	Length of guard interval	12 samples
Receiver parameters	Frequency offset between the transmitter laser and local oscillator	0 MHz
	Photodiode responsivity	0.6 A/W
	Thermal noise power density	100 $pA/Hz^{1/2}$
	Electrical filter bandwidth	3 GHz
	Electrical filter profile	4^{th}-order Bessel
	OBPF bandwidth	12 GHz [optimal: 8-10 GHz for 7-channel-superchannel]
	OBPF resolution	2 GHz

2.5 Nyquist FDM (NFDM) transceiver

In this section, we evaluate Nyquist frequency division multiplexing (NFDM), where, in contrast to NWDM, DSP-based electronic multiplexing is carried out to achieve non-overlapping spectra by modulating a large number of electrical subcarriers with sinc-shaped pulses before transmission through the optical channel. This technique is also in contrast to eOFDM, where an optical channel consists of a group of sinc-shaped overlapping spectra, as we saw in the previous sections. An advantage of NFDM is that guard intervals are not needed for CD compensation. However, as in eOFDM, pilot tones can be used for carrier phase recovery and equalization.

2.5.1 NFDM transmitter model

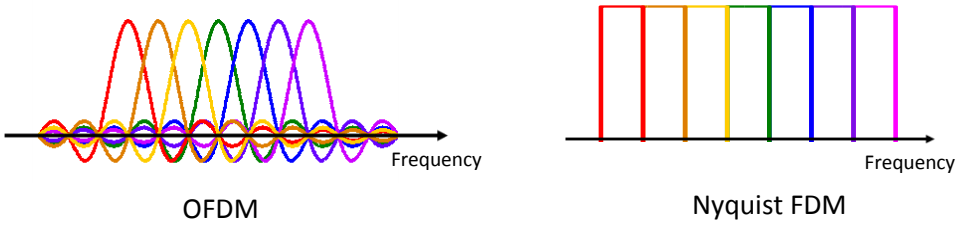

Figure 2.27 – Spectral profiles of OFDM and NFDM

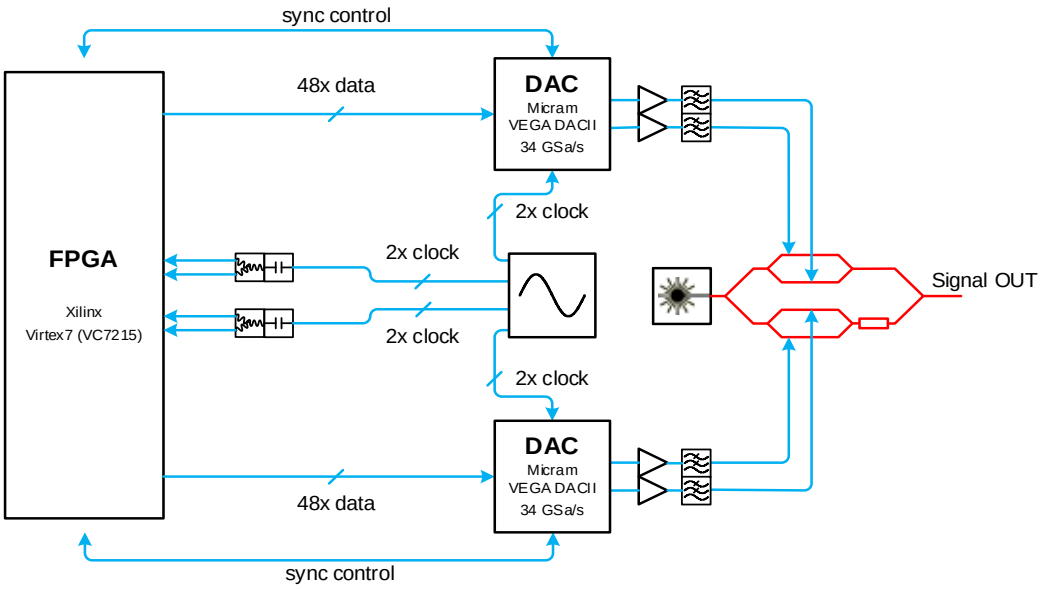

Figure 2.28 – NFDM transmitter design

The hardware transmitter setup of electrical NFDM is the same as the conventional OFDM and eFOFDM. However, NFDM uses a rectangular function to realize the channel orthogonality (see Figure 2.27) [11-13]. To realize this spectral profile in the implementation, additional filtering is required as illustrated in Figure 2.29.

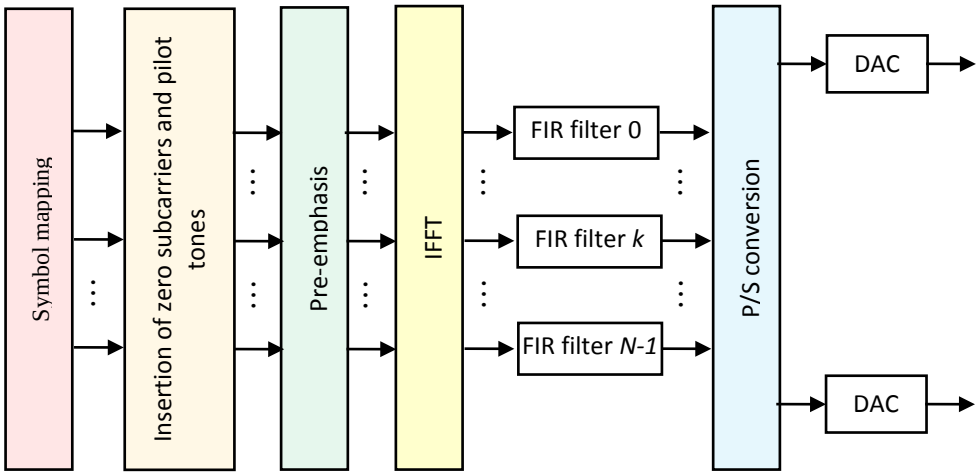

Figure 2.29 – DSP procedure of NFDM

The DSP in NFDM is as follows: the inverse fast discrete Fourier transform (IDFT) is used to multiplex the subcarriers with 256 points. 16QAM formats are used for NFDM data modulation, and the subcarriers in the high-frequency region are zero-padded to avoid aliasing. The number of zero-padded subcarriers is either 20 or 40, corresponding to 1 GHz or 2 GHz guard band between channels. The mapped signal is pre-emphasized to equalize the sinc-function roll-off during digital-to-analogue conversion and the analogue bandwidth of the digital-to-analogue converter (DAC). After IFFT, finite impulse response filters are used to create the rectangular signal spectral profile. In principle, the filter for pulse shaping is applied in series and has a sinc-function spectral profile. In , we apply the filters in parallel to relax the implementation complexity before the signal is parallel to serial converted. The manipulations of the parallel filters will be described later. The NFDM signals are then converted to analogue signals using 12.5-GS/s digital-to-analogue converters. Low-pass filters are applied to filter out the aliasing. The bandwidth of the aliasing filter is 6.25 GHz and the spectral profile is 8^{th}-order Gaussian. The signals are amplified by electronic drivers and modulated onto each optical carrier. The input electrical signal power into the modulators is -12 dB with respect to V_π^2. In the optical domain, seven channels are used with channel spacing of 12.5 GHz.

Next, we will provide the impulse response of the pulse-shaping FIR filters 0…*N*-1. Let us assume that $a_{i,n}$ is the frequency-domain n^{th} subcarrier data in the i^{th} OFDM symbol. Firstly, let us recall the time-domain signal in conventional OFDM:

$$s(i\cdot N+k)=\sum_{n=0}^{N-1}a_{i,n}\exp(2\pi j(i\cdot N+k)\cdot n/N)=s_{i,k}\qquad k=0,1\ldots N-1 \tag{2.1}$$

where *N* is the number of subcarriers. In NFDM, where the impulse response of the pulse-shaping filter in serial is represented by *h*(*k*), the time-domain signal of NFDM is a sinc-function and may overlap, so Eq. (2.1) has to be generalized as:

$$\begin{aligned}s(i\cdot N+k)&=\sum_{p=-\infty}^{+\infty}\sum_{n=0}^{N-1}a_{p,n}\exp(2\pi j(p\cdot N+k)\cdot n/N)\cdot h(i\cdot N+k-p\cdot N)\\&=\sum_{p=-\infty}^{+\infty}h(i\cdot N+k-p\cdot N)\cdot\sum_{n=0}^{N-1}a_{p,n}\exp(2\pi j(p\cdot N+k)\cdot n/N)\\&=\sum_{p=-\infty}^{+\infty}h(i\cdot N+k-p\cdot N)\cdot s_{p,k}\qquad k=0,1\ldots N-1\end{aligned} \tag{2.2}$$

From Eq. (2.2), it can be seen that the impulse response of the FIR filter *k* in is the k^{th} tributary demultiplexed, by a factor of *N*, from *h*(*k*), *h*(*i*·*N*+*k*-*p*·*N*), -∞ < *p* < +∞. The complexity for pulse shaping is also reduced by a factor of *N* when compared to the serial implementation.

2.5.2 NFDM receiver model and set-up

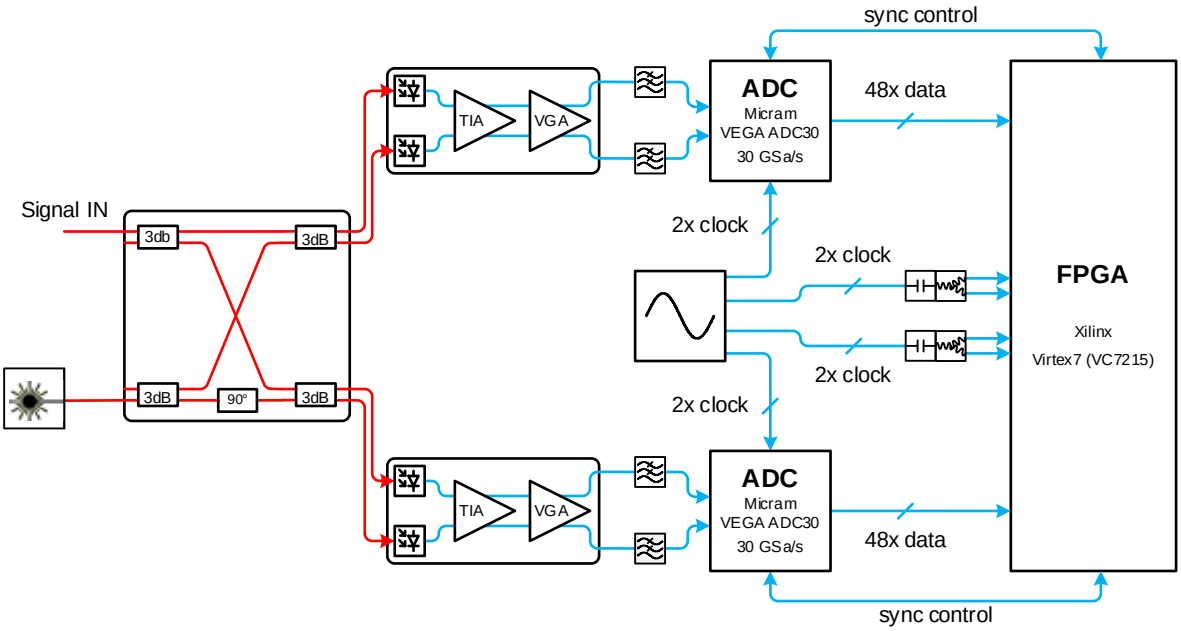

Figure 2.30 – NWDM receiver design

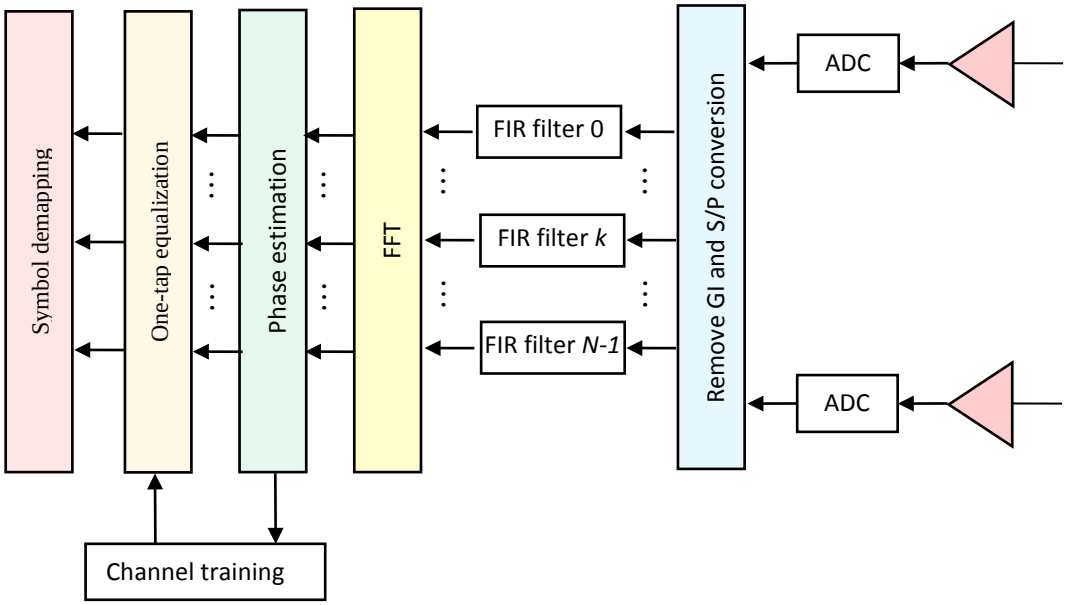

Figure 2.31 – DSP procedure at the receiver for NFDM decoding

The receiver setup is the same as Figure 2.10 while the DSP procedure for NFDM is illustrated in Figure 2.31. The powers of the local oscillator and the received signal are 10 dBm and 0 dBm respectively, and their polarizations are controlled to be the same. The equivalent thermal noise spectral power density of the detectors is 100pA/Hz$^{1/2}$ and the responsivity of photodiodes is 0.6 A/W. After detection, the signals are electrically amplified and filtered by 4th-order Bessel electrical filters with 3-GHz bandwidth. The received analogue signals are sampled by ADCs and decoded using DSP algorithms. Each NFDM symbol is serial-to-parallel converted, filtered by FIR filters that are matched to

those at the transmitter. Then FFT is applied to transform the time-domain signal to the frequency domain. Note that due to non-overlapped spectral profiles, no guard interval is required in NFDM. Channel is estimated based on the time-domain averaging algorithm. After channel equalization, the symbols are de-mapped and bit error rate is calculated using direct error counting.

2.5.3 Performance results

In NFDM, it is essential to filter the spectral profile to be rectangular to maintain the channel orthogonality. Firstly, we investigate the single-channel case to clarify this issue. Figure 2.32 shows the performance of single optical channel N-FDM (256 electrical subcarriers) versus the memory length of the FIR filter at 12.5 dB OSNR. Because NFDM tries to create a rectangular spectral profile or a sinc-function in the time domain and the sinc function has very long tails, a large memory length is required for the FIR filter. The figure shows that even when the memory length is increased to 40, the performance is still only at around a BER of 1×10^{-3}. This performance is poorer when compared to conventional OFDM and eFOFDM. Further increasing the memory may improve the performance gradually but increases the implementation complexity. In the following, we will assume that the memory length is 40.

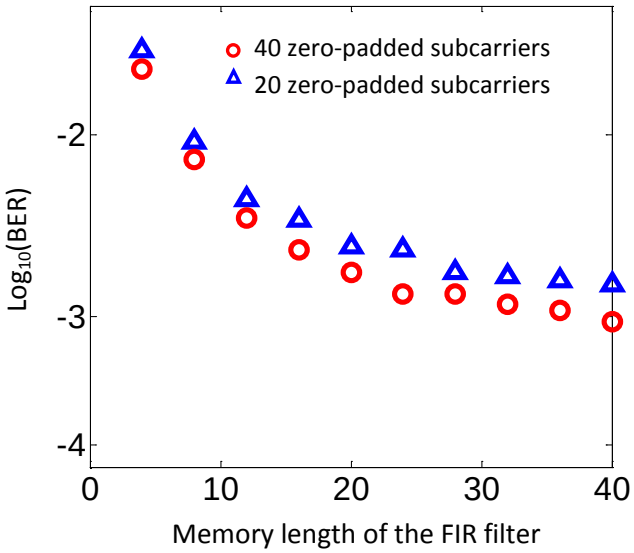

Figure 2.32 – Performance versus the memory length of the FIR filter

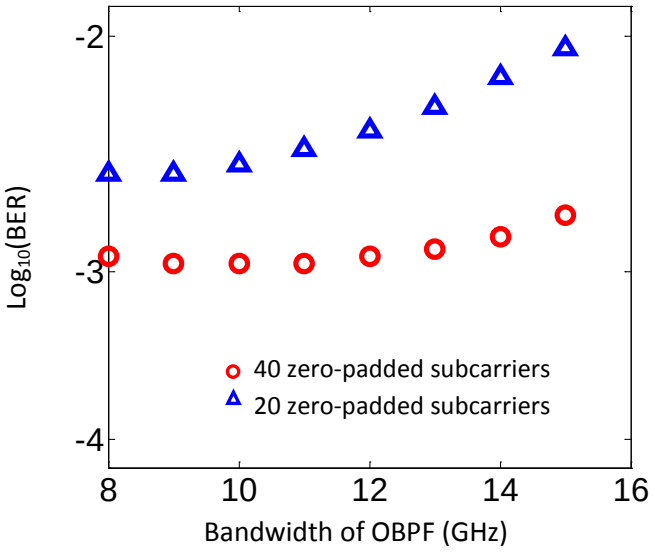

Figure 2.33 – Performance versus the bandwidth of the OBPF (2-GHz resolution)

Figure 2.33 shows the performance versus the bandwidth of OBPF in a seven-channel super-channel scenario. It can be seen that the trend is similar to those of conventional eOFDM and eFOFDM in Figure 2.19 and Figure 2.32. However, the performance is degraded because rectangular spectral cannot be ideally realized and crosstalk exists between electrical subcarriers. Figure 2.34 compares the BER performance with different guard bands in the single-channel and super-channel scenarios. Similar to conventional eOFDM and eFOFDM, under the optimized system performance and using 40 zero-padded subcarriers (2-GHz guard band), the super-channel performance is very similar to the single-channel case. When the guard band decreases to 1 GHz, the performance using seven-channels is degraded and error floor is observed.

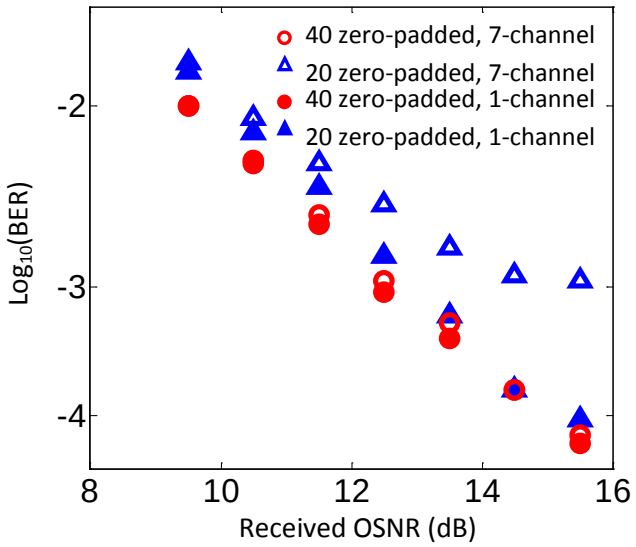

Figure 2.34 – Performance versus the received OSNR for single and seven channel cases

2.5.4 Design parameters

Table 2.4 – N-FDM design parameters.

Transmitter parameters	Optical channel number	7
	Modulation format	16QAM
	Total FDM subcarrier number	256
	Zero-padded subcarrier number	20/40
	DAC sampling rate	12.5 GS/s
	Channel spacing	12.5 GHz
	Bandwidth of the aliasing filter	6.25 GHz
	Spectral profile of the aliasing filter	8^{th}-order Gaussian
	Normalized power into the modulator	-12 dB
	Memory length for pulse shaping	40 (Optimal >40)
	Length of guard interval	0
Receiver parameters	Frequency offset between the transmitter laser and local oscillator	0 MHz
	Photodiode responsivity	0.6 A/W
	Thermal noise power density	100 pA/$Hz^{1/2}$
	Electrical filter bandwidth	3 GHz
	Electrical filter profile	4^{th}-order Bessel
	OBPF bandwidth	12 GHz [optimal: 8-10 GHz for 7-channel-superchannel]
	OBPF resolution	2 GHz

2.6 Discussion

In this section, we have investigated the super-channel transceiver design of eOFDM, eFOFDM, and NFDM. These formats have similar hardware implementation setups in terms of transmitter and receiver, and the key difference lies in the DSP encoding and decoding. eOFDM and eFOFDM are both based on sinc-function spectral profiles and can be implemented using computationally efficient FFT and DCT respectively. To enable dispersion compensation using single-tap equalizers, cyclic and symmetric extension based GIs are required in eOFDM and FOFDM, which however would reduce the net data rate for long distance transmission. On the other hand, NFDM is based on a rectangular spectral profile and requires additional filtering in the DSP implementation. In the time-domain, a sinc-function pulse shape is created by using FIR filters. Due to the long tails of the sinc function, a large memory length of 40 taps or longer is required. At a memory length of 40, the result shows that NFDM still exhibits performance penalty compared to eOFDM and eFOFDM (see Table 2.5). The advantage of NFDM is that the spectrum of channels does not overlap in the frequency domain so GI is not required for dispersion compensation.

Table 2.5 – Summary of results of back-to-back performance studies carried out for the electrical multiplexing schemes. All studies examined the cases of 20 and 40 zero-padded subcarriers (SC), equivalent to 1-GHz and 2-GHz guard band between flex-channels, respectively.

BER vs.	eOFDM	eFOFDM	N-FDM
Single channel			
FIR filter memory length	-	-	40 taps for BER=10^{-3} with 40 SC. With 20 SC, BER slightly above 10^{-3}. (Figure 2.32)
Rx OSNR (with optimised design parameters)	BER ~ 10^{-4} for OSNR = 12.5 dB with 40 SC BER ~ $10^{-3.5}$ for OSNR = 12.5 dB with 20 SC (Figure 2.17, Figure 2.21)	BER ~ 10^{-4} for OSNR = 12.5 dB with 40 SC BER ~ $10^{-3.2}$ for OSNR = 12.5 dB with 20 SC (Figure 2.26)	BER ~ 10^{-3} for OSNR = 12.5 dB with 40 SC BER ~ 10^{-3} for OSNR = 13 dB with 20 SC (Figure 2.34)
Seven-channel super-channel			
Rx OBPF bandwidth	For BW = 8-15 GHz BER < 10^{-3} with 40 SC For BW = 9-10 GHz BER ~ 10^{-3} (or slightly higher) with 20 SC (Figure 2.19)	For BW = 8-15 GHz BER < 10^{-3} with 40 SC For BW = 8-9 GHz BER ~ 10^{-3} (or slightly higher) with 20 SC (Figure 2.25)	For BW = 9-11 GHz BER ~ 10^{-3} with 40 SC BER > 10^{-3} with 20 SC (Figure 2.33)
Rx OSNR (with optimised design parameters)	BER ~ 10^{-4} for OSNR = 12.5 dB with 40 SC BER ~ 10^{-3} for OSNR > 13.5 dB with 20 SC (error floor observed) (Figure 2.21)	BER ~ 10^{-4} for OSNR = 12.5 dB with 40 SC BER ~ 10^{-3} for OSNR > 13.5 dB with 20 SC (error floor observed) (Figure 2.26)	BER ~ 10^{-3} for OSNR = 12.5 dB with 40 SC BER ~ 10^{-3} for OSNR > 14.5 dB with 20 SC (error floor observed) (Figure 2.34)

3 Description of switching node models

This chapter sums up the switching node implementations analysed in T4.1 and T4.2 and reported in D4.3 and D4.5. It focuses on the design and parameters needed to carry out the simulations to investigate the performance of the node for each of the transceiver solutions evaluated in Section 0.

Relying on the hierarchical topology depicted in Figure 1.1, at the **fibre link level**, a WSS selects a super-channel that contains the flex-channels to be dropped locally. For a correct operation, the node also needs optical amplification and channel monitoring. Two configurations for the FOX-C node have been considered:

The first arrangement is based on a single low port count WSS offering flexible grid operation and the utilization of the fibre ports for both add and drop functions via a circulator, which implies the same wavelength super-channel must be added and dropped (see Figure 3.1). This architecture is optimally suited for in-line ROADM nodes.

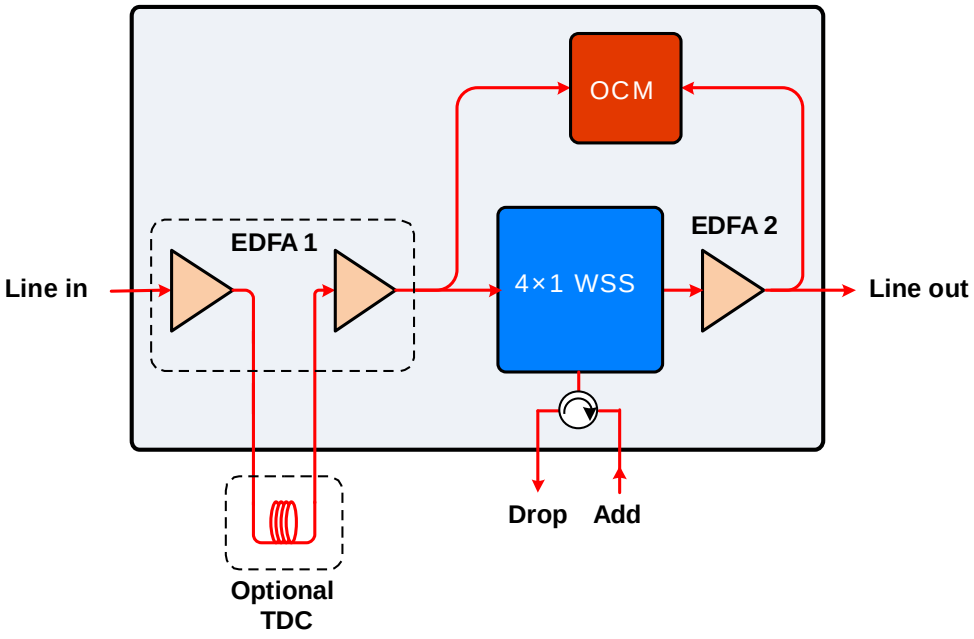

Figure 3.1 – First arrangement for a FOX-C superchannel Add/Drop node based on a single WSS used bi-directinoally. Accompanying amplification and monitoring is also depicted.

The second arrangement is based on two 1×9 WSS offering flexible grid operation with these WSS assigned to a network direction (inbound and outbound traffic on a node link), as can be seen in Figure 3.2. This arrangement provides greater functionality, which can be exploited for flexible optical cross-connects where several links converge.

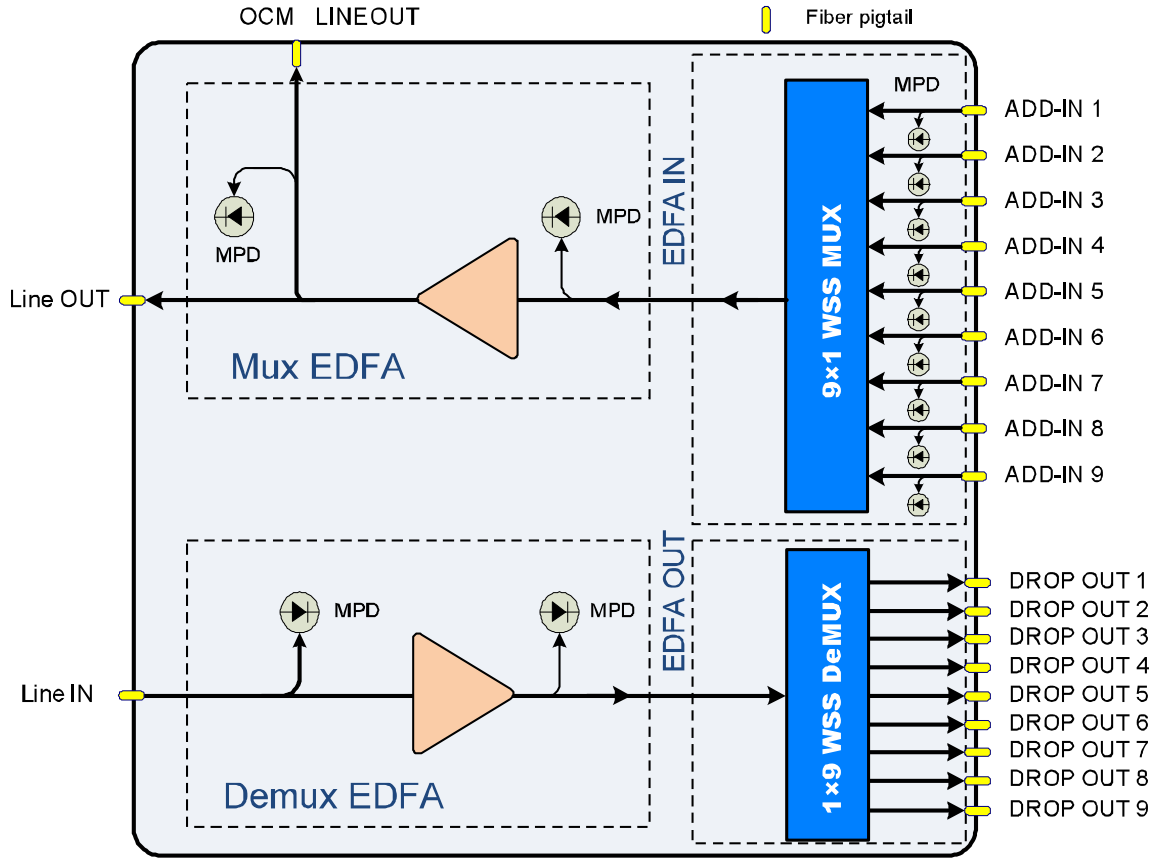

Figure 3.2 – Second arrangement for a FOX-C superchannel Add/Drop node based on a dual WSS arrangement, where one is used to distribute the incoming channel across the drop ports and the other for aggregating the channels towards the line side.

On the other hand, at the **super-channel level**, several technologies have to be implemented for the different types of signal formats discussed in Section 0.

For the OFDM-based multi-band schemes, matched filtering conditions are required for the clear extraction (i.e. both drop and erase), while for the add function, a novel phase regeneration stage has been proposed in the FOX-C project consisting of a wave synchronization and a phase regeneration stage. The former stage creates a phase-synchronised and coherent reference signal from the through orthogonal bands which are then used in the latter stage to regenerate the phase of the newly added signal(s) with respect to the existing carriers.

For the Nyquist-FDM scheme, an optimum combination of ultra-fine filter selectivity with minimum guard band requirements is needed. The fine sub-superchannel selector elements must be bandwidth adaptable to the spectral width of the flex-channels. Therefore a high resolution (around 1GHz) adaptive optical filter is required, allowing a detailed design of the filter response function. This filter is used in the drop part of the node and also in the add part to equalise and pre-shape the added band.

In the next two sections these two filter models, namely a high resolution filter for non-overlapping flex-channels such as those generated by N-FDM transceivers and an all-optical interferometric filter for overlapping flex-channels such as those generated by AO-OFDM transceivers, will be described and a list of their design parameters will be provided.

3.1 High spectral resolution filter based add/drop node

Section 2 only considers the design of the transceiver and does not take the effect of channel add/drop into consideration. In this section, we will extend the point-to-point setup and provide the network configuration under study. Figure 3.3 shows the system setup. Seven-channel

eOFDM/eFOFDM/NFDM signals are generated by transmitters as designed in the last section. The signals pass through spans of fibers with 80-km single-mode fiber per span with 0.2 dB/km loss and 17 ps/nm/km dispersion. At the network node, the central channel (the fourth channel) is dropped using a high spectral resolution filter and detected using a coherent receiver as discussed in the last section. Another signal is generated and added to the fourth channel in the network node using the second high spectral resolution filter. Then the combined signals pass through another fiber link with spans of 80-km single-mode fiber. At the final destination, the signals in the super-channels are demultiplexed using a high spectral resolution filter and detected using coherent receivers. In section 4, we will focus on the investigation of performance for the following three signals: the dropped fourth channel, the added fourth channel at the final destination and the fifth channel at the final destination. In this section, we will provide the model of the high spectral resolution filter for add/drop in the eOFDM/eFOFDM/NFDM super-channels.

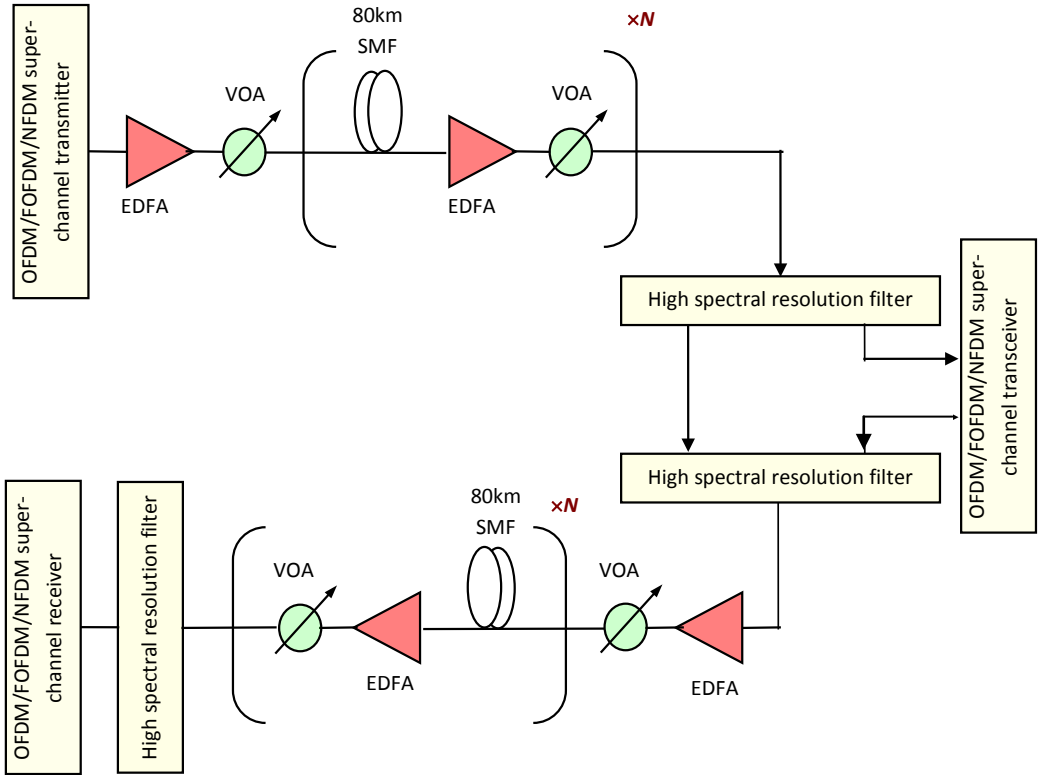

Figure 3.3 – Setup of the super-channels in the network configuration with channel add/drop.

When each channel is modulated using eOFDM/eFOFDM/NFDM signals, the optical spectrum of each channel is near-rectangular without spectral overlap. Figure 3.4, Figure 3.5 and Figure 3.6 show the sketched spectra of eOFDM/eFOFDM/NFDM super-channels, respectively. To drop each optical channel, a near-rectangular filter is used. In this system, the rolloff of the filter should be as sharp as possible to achieve the minimized guard band between channels. The FOX-C project proposes the design and development of novel adaptive filtering elements with ultra-fine resolution below 1GHz over the superchannel bandwidth. Such fine resolution allows for matched design of adaptive optical filters to be used as channel selectors.

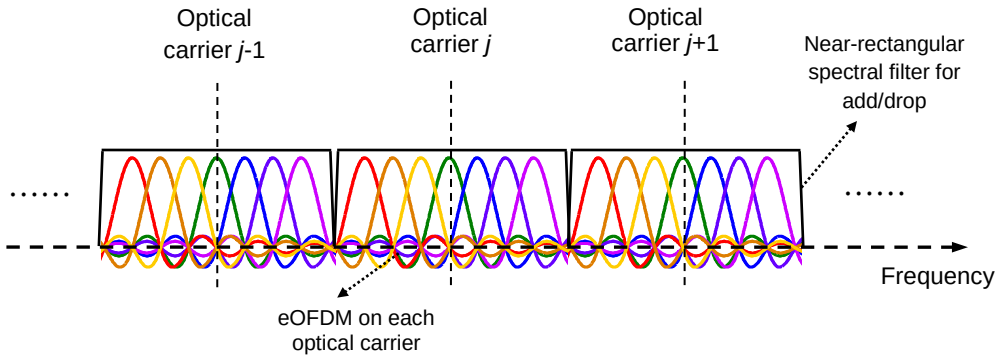

Figure 3.4 – Optical super-channel with each optical carrier modulated by an eOFDM signal and multiplexed using the N-WDM approach.

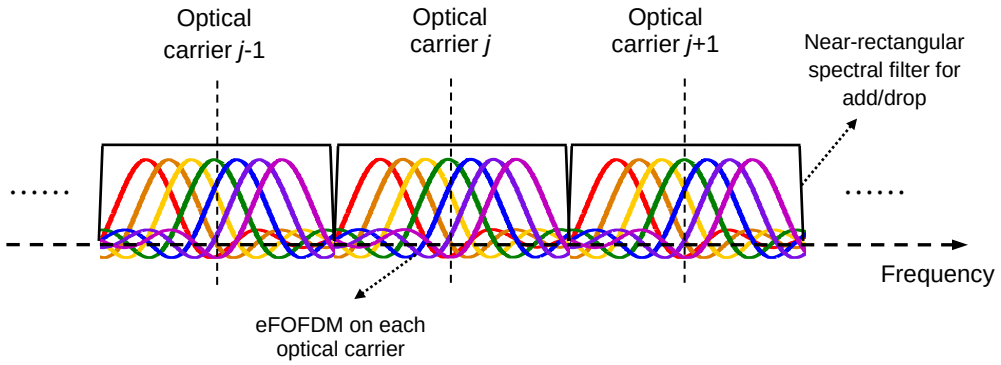

Figure 3.5 – Optical super-channel with each optical carrier modulated by an eFOFDM signal and multiplexed using the N-WDM approach.

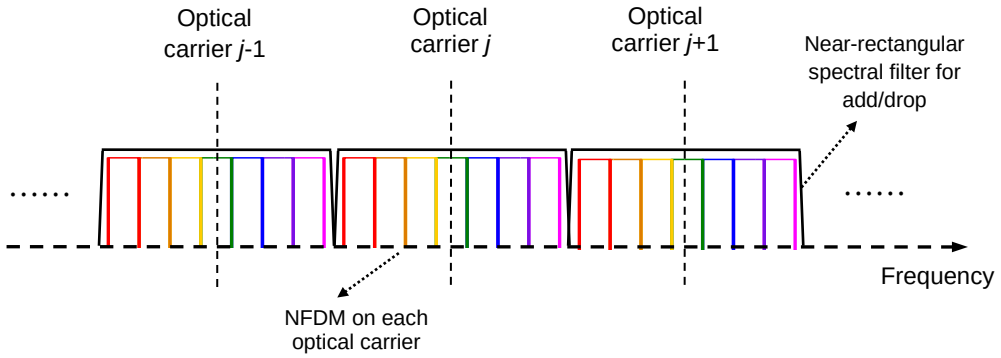

Figure 3.6 – Optical super-channel with each optical carrier modulated by an NFDM signal and multiplexed using the N-WDM approach.

3.1.1 Model of the high spectral resolution filters and design parameters

The fine resolution filter elements will be developed on a hybrid free-space/guided-wave optics platform. This solution has been originally investigated as a platform for developing wavelength selective switches (WSS) for DWDM networking applications, consisting of means for spatial dispersion and for switching via spatial light modulators. However, conventional WSS devices are designed for a chosen WDM channel plan and use custom pixel arrays matching the channel layout, created in either MEMS tilting mirrors [14] or liquid-crystal polarization rotation [15] technology. Replacing the active switching element by a high-density pixel array implemented in LCoS technology allows for finer (in-band) spectral access and modulation. This enables flexible channel plans and programmable bandwidth

filters in WSS applications. A WSS can be made more compact by using a waveguide grating router (WGR) as the dispersive element [16], instead of bulk gratings. By engineering the dispersive properties of the WGR, the resolving power can be made much finer in a narrower spectral range, allowing for high resolution access to in-band spectral components. A spectral photonic processor with 3 GHz bandwidth was realized by tailoring the dispersion to span 100 GHz bandwidth only [17]. Within the FOX-C project we expect to go beyond the state of the art by targeting a resolution of 800 MHz (defined as the 3-dB roll-off at a sharp edge). The specific implementation that will be realized will utilize two WGR that are vertically stacked (along with an implementation of polarization diversity on account of the LCoS device and possible polarization-dependent wavelength shift due to waveguide birefringence), free-space imaging lens and the LCoS spatial light modulator (SLM), see Figure 3.7. One WGR disperses the input signal, which is made incident on the LCoS SLM, reflecting the signal back to the second WGR which recombines the spectral components after they have been modified by the LCoS function. This solution eliminates the need for a circulator when using a single WGR, a solution that is prone to back-reflection. Filter adaptability will be computer-controlled by commands issued to the LCoS SLM. Power consumption is expected to be minimal and attributed primarily to the computer (or controller) running the LCoS modulator.

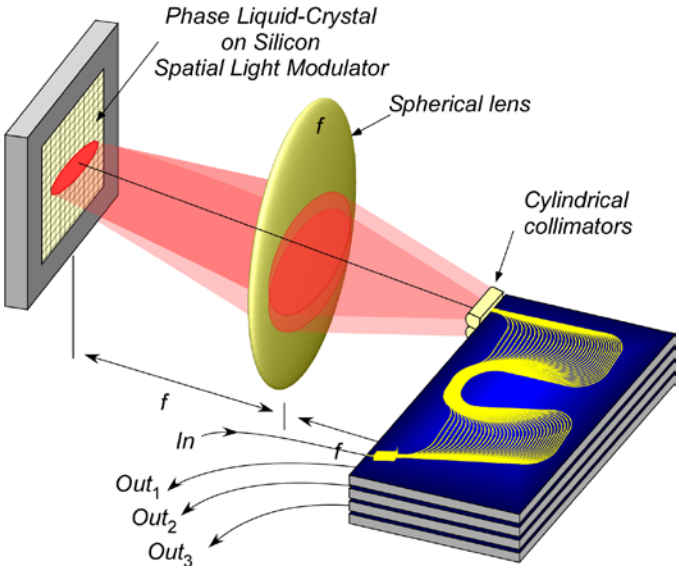

Figure 3.7 – Layout of the technology platform for the high spectral resolution filter

Mathematically, the high spectral resolution filters can be modeled as the convolution of the desirable ideal filter with a Gaussian function whose spectral bandwidth is determined by the resolution:

$$H(f) = H_{ideal}(f) \otimes H_r(f) \tag{3.1}$$

$$H_r(f) \propto \exp(-(f \cdot \sqrt{2} / resolution)^2 / 2) \tag{3.2}$$

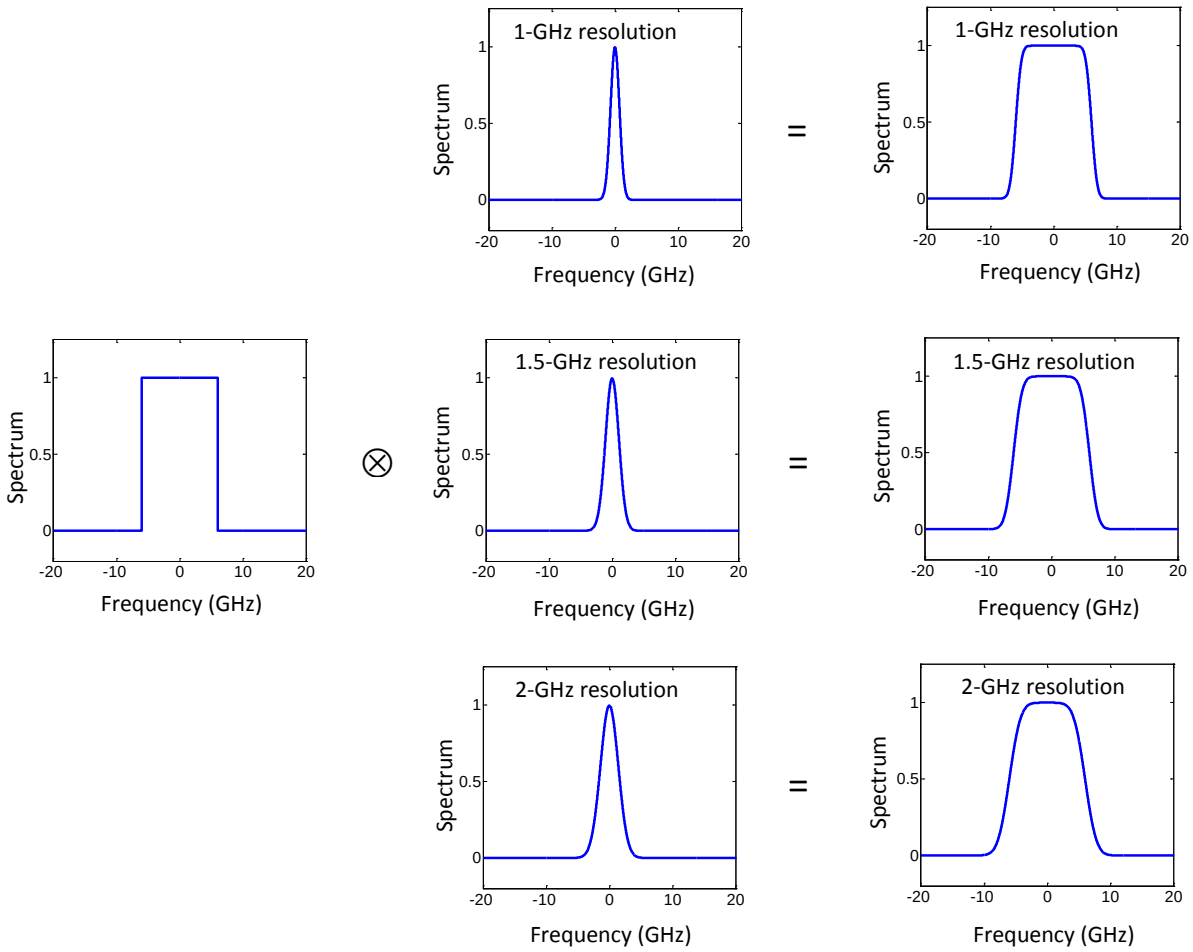

Figure 3.8 – The first column: the desirable filter profile; The second column is the Gaussian function with 1, 1.5 and 2 GHz resolution; The right column represent the practically realized transfer function of high spectral resolution filter under 1, 1.5 and 2 GHz resolution.

Figure 3.8 shows the procedure to realize the practical transfer function of the high spectral resolution filter. It can be seen that the finer the resolution, the sharper the filter spectral edge. In order to filter out the eOFDM/eFOFDM/NFDM signals with minimized crosstalk, a finer resolution optical filter is desirable. These filter profiles will be used in the next chapter to investigate the add/drop performance.

The high-resolution filter is likely to have high losses. Two different scenarios have been considered for the complete add/drop node design: one with the filter **at a loss of 12dB and the other at a loss of 22dB. For these scenarios, in WP4, the node design together with compensating amplification as well as signal powers at different stages have been evaluated, based on target received power at the node (-2dBm over the C-band) and transmit power levels (+20dBm over the C-band).**

3.2 All-Optical Interferometric node

3.2.1 The AO Interferometric node model and set-up

The proposed architecture for the add-drop multiplexing of OFDM subcarriers within a super-channel is shown in the detailed diagram depicted in Figure 3.9Figure 3.8. A list of the corresponding components is presented in Table 3.1.

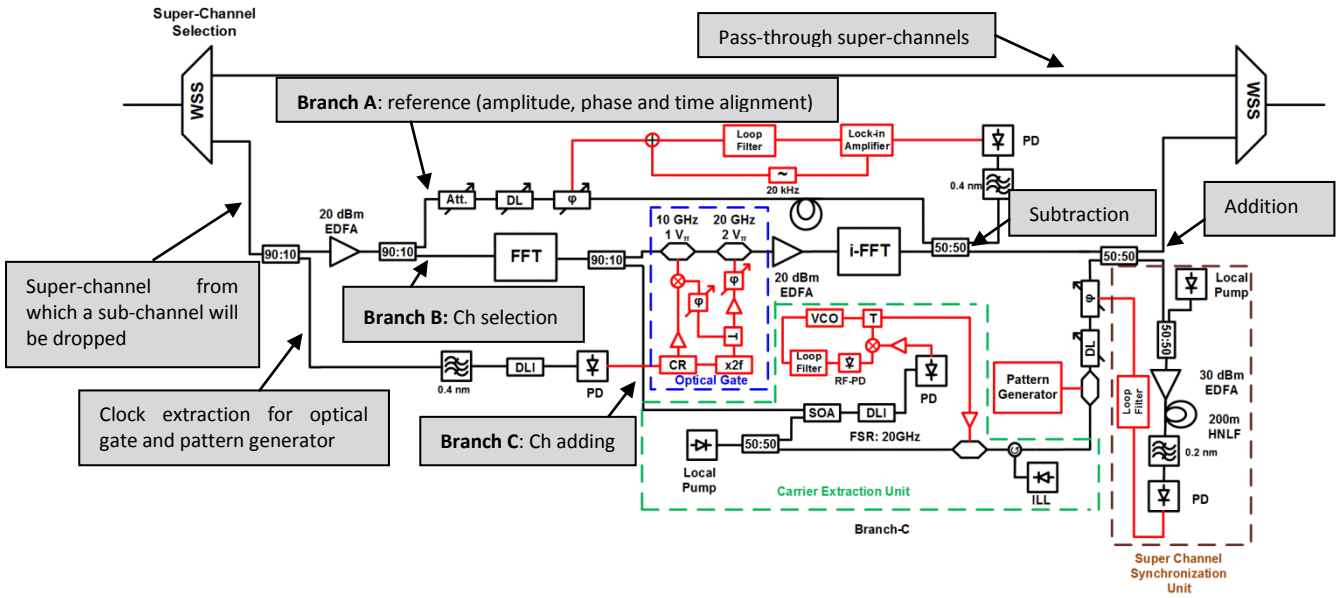

Figure 3.9 – Detailed diagram of the setup of the AO interferometric node

Two state-of-the-art WSS units perform the super-channel selection. A small percentage of the signal power is tapped from one of the outputs of the first WSS and used for extracting the clock for the synchronization of the optical gate and the pattern generator. For the clock extraction process a single sub-channel is selected by a band-pass filter of 0.4 nm and its phase-encoded signal is subsequently converted to an amplitude waveform by a delay interferometer filter prior to detection by a high speed photodiode.

The interferometer to which this AO interferometric node model alludes encompasses branches A and B shown in Figure 3.9, which are used for channel selection and subtraction. Branch A can be regarded as a reference path that only introduces amplitude, phase and timing alignment to the OFDM signal. Branch B, on the other hand, is responsible for the replication of the sub-channel that is to be erased. This is accomplished through optical FFT/iFFT processes and optical sampling carried out by an optical gate primarily composed of two optical amplitude modulators. The signal waveform generated at this branch is subtracted from the OFDM signal propagating at branch A. On a technical note, it is important to have only one EDFA at branch B (to minimise the loss) and for the optical path of each FFT/iFFT filter to remain below 10 m (to keep environmentally induced phase drifts to a minimum). However, a stabilization unit is still required to compensate for any (however small) induced phase variation and ensure the conditions of destructive interference between the two branches of the interferometer are met.

Finally, a small percentage of the power of the signal travelling along branch B is tapped after the FFT unit and conducted to branch C, where the optical carrier is extracted through four-wave mixing in an SOA followed by injection locking of the local laser of the transmitter for the new channel to be added.

3.2.2 Design parameters

Table 3.1 – AO interferometric node design parameters.

Device	#	Characteristics
FFT processors & WSSs for super- channel selection		
FFT	1	10 GHz sinc transfer function 6 dB losses Optical Path length : 10 m (max)

iFFT	1	10 GHz sinc transfer function 6 dB losses Optical Path length : 10 m (max)
WSS	2	Reconfigurable band-pass filters over the C band, grid-less operation 6 dB losses
Optical Gate		
Amplitude Modulator	2	Avanex SD 40 Bandwidth 33 GHz
20 GHz Clock Amplifier	1	~2 $V_{RF,PI}$
Frequency Doubler	1	10 to 20 GHz
Broadband Amplifier	1	~1 $V_{RF,PI}$
RF Delay Line	3	> 100 ps
RF Mixer	1	10x20GHz Mixer
High Speed PD	1	>10 GHz
Clock Recovery Module	1	10 GHz
Synchronization & Interferometer Stabilization		
Low Speed PD	2	35 MHz Bandwidth Pre-amplified
Lock-in Amplifier	1	
Clock source	1	~20 kHz
Loop Filter	2	Low pass filter
Tunable Laser	1	Local pump
High Power EDFA	1	> 30dBm output
Highly Nonlinear Fiber	1	200m
Narrow Filter	3	0.4nm & 0.2nm
Carrier Extraction Unit		
SOA	1	
Tunable Laser	1	Optical Pump
Injection Locking Laser	1	
VCO	1	20 GHz
RF Mixer	1	Broadband

RF Coupler	1	
Broadband Amplifier	2	>30 GHz
High Speed PD	1	>30GHz
DLI	1	20 GHz
Intensity Modulator	1	> 30 GHz
Additional Devices		
Optical Delay Line	2	> 100 ps
Optical Phase Control	2	Fibre stretcher using PZT crystals
PPG Transmitter	1	New data – Identical Baudrate Clock from Clock Recovery Unit
Data Modulator	1	
Optical Amplifier	2	>20 dBm

4 System performance estimation studies and results

This chapter reports on the results of the simulations conducted in T2.2 to estimate the performance of the switching node models described in Section 3. In this version of the document only the high spectral resolution (HSR) filter based node is taken into consideration and the network configuration under study is that depicted in Figure 3.3. Likewise, only the performance of the electronic transceiver schemes for the generation of the super-channel is analysed.

4.1 Switching node performance for different transmission schemes

4.1.1 HSR filter based node performance for eOFDM signals

In this section, we will use the simulation setup in Figure 3.3 to investigate the performance of eOFDM-based optical super-channels taking into account both the transceiver design and the node design. We will measure the BER of three channels: the dropped channel (the fourth channel) at the network node; the added channel (into the fourth channel) that is detected at the final destination; and the fifth channel that passes through the network node and is detected at the final destination.

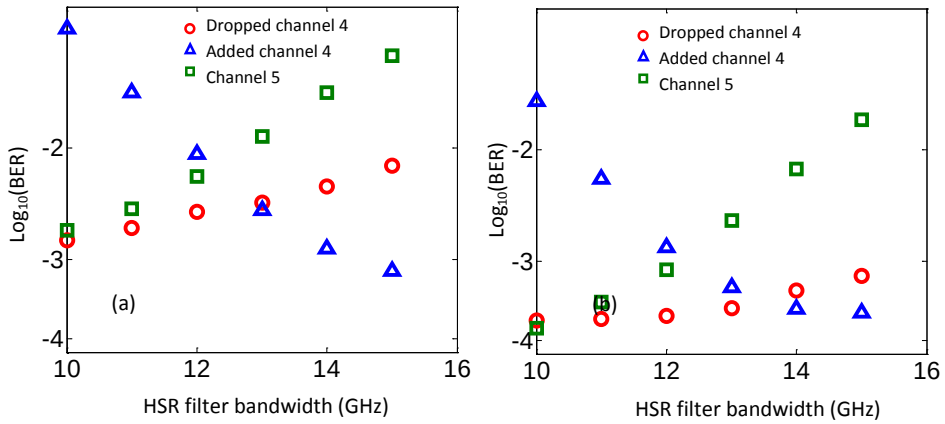

Figure 4.1 – Performance versus the bandwidth of the HSR filter with 2-GHz resolution at 12.5-dB OSNR (per channel) when the guard band between channels is (a) 1 GHz and (b) 2 GHz.

Figure 4.1 shows the performance sensitivity to the bandwidth of the HSR filter. For the dropped channel 4 at the network node, the performance variation is similar to Figure 2.19. When the bandwidth is higher than 10 GHz, the performance is gradually degraded due to the optical noise. For the added channel 4, when the HSR filter bandwidth is small, there is residual power left from the dropped channel at the spectral band of the fourth channel. This residual power would introduce crosstalk to the added channel 4. The crosstalk reduces as the bandwidth of the HSR filter increases, resulting in improved performance for the added channel. However, when the bandwidth of the HSR filter is large, the power from the adjacent channel, channel 5, is also filtered out by the HSR filter at the network node. Consequently, the performance of the channel 5 degrades significantly as the bandwidth increases. Clearly, there is an optimal filter bandwidth that balances the performance of these channels and is around 12 GHz. Note that this bandwidth is slightly larger than the optimal bandwidth when only channel 4 is considered (~10 GHz) as illustrated in Figure 2.19.

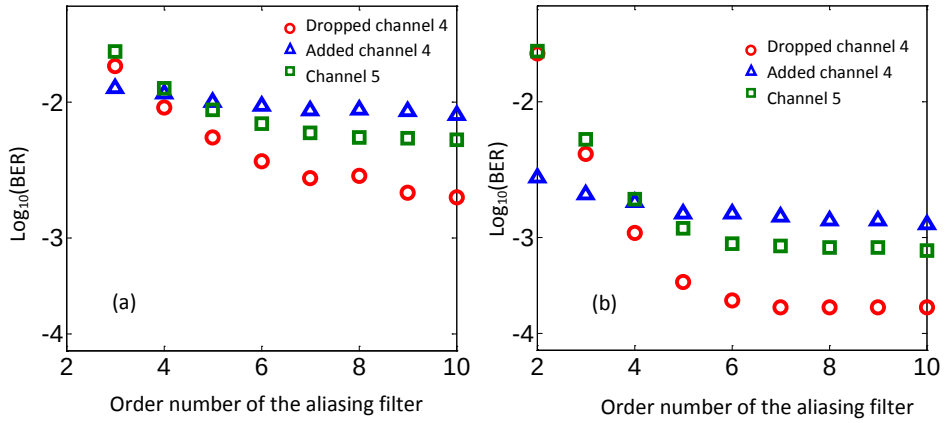

Figure 4.2 – Performance versus the order number of the aliasing filter for the dropped channel 4, added channel 4, and channel 5 when the guard band between channels is (a) 1 GHz and (b) 2 GHz.

Under the optimized HSR filter bandwidth (12 GHz), we investigate the performance versus the order number of the aliasing filter and the results are shown in Figure 4.2. As expected, the performance highly depends on the roll-off of the aliasing filter to avoid the crosstalk between channels and, for both cases, a Gaussian-shaped aliasing filter of more than 6th order is required to attain the near-optimum performance. It is also observed that, when the guard band is 1 GHz, the system is very sensitive to the crosstalk and 1×10^{-3} cannot be reached.

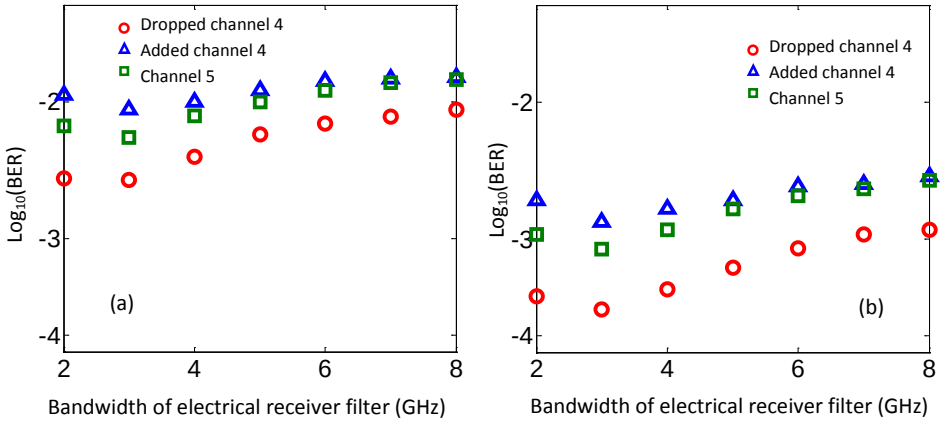

Figure 4.3 – Performance versus the bandwidth of the receiver electrical filter for the dropped channel 4, added channel 4, and channel 5 when the guard band between channels is (a) 1 GHz and (b) 2 GHz.

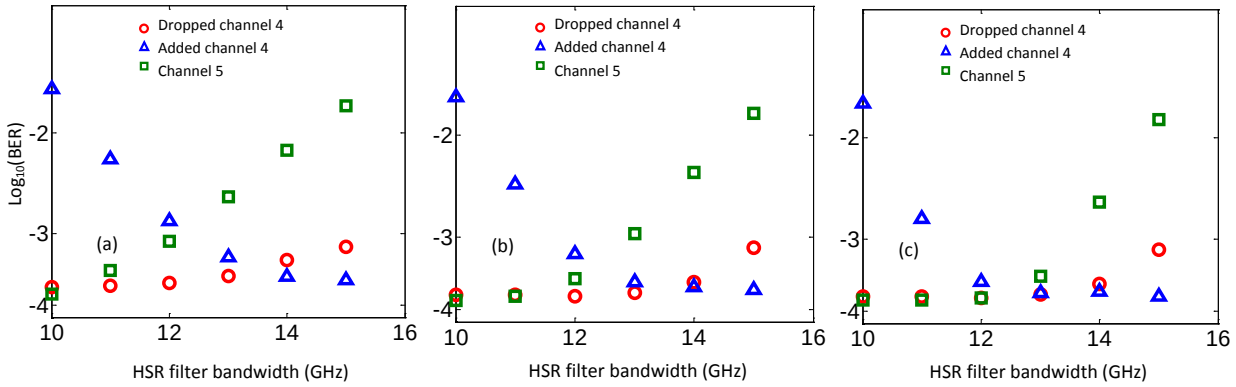

Figure 4.4 – Performance versus the bandwidth of the HSR filter at 12.5-dB OSNR (per channel) and 2-GHz guard band when the filter resolution is (a) 2 GHz (b) 1.5 GHz and (c) 1 GHz.

Figure 4.3 further investigates the performance as a function of the bandwidth of the electrical receiver filter under optimized HSR filter bandwidth (12 GHz) and 8th-order Gaussian aliasing filter. Because the balance on the crosstalk between channels has been realized by the optical filter, the performance is not very sensitive to the electrical filter bandwidth. Unless the filter bandwidth is too narrow when the ISI is induced, the BER only slightly increases as the bandwidth increases.

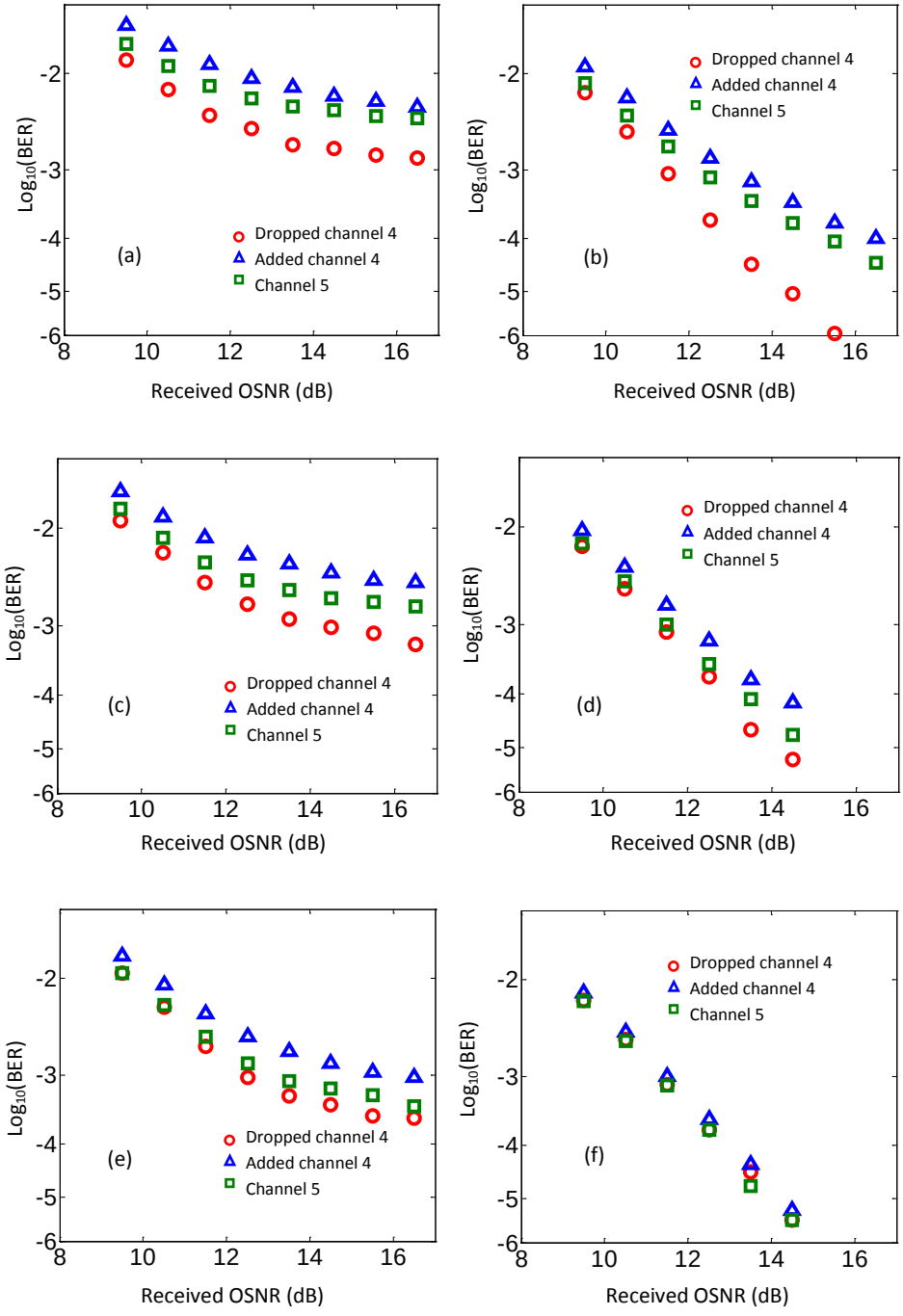

Figure 4.5 – Performance versus the received OSNR (a) 1-GHz guard band and 2-GHz resolution; (b) 2-GHz guard band and 2-GHz resolution; (c) 1-GHz guard band and 1.5-GHz resolution; (d) 2-GHz guard band and 1.5-GHz resolution; (e) 1-GHz guard band and 1-GHz resolution, and (f) 2-GHz guard band and 1-GHz resolution.

All of the above investigations are based on the HSR filter with 2-GHz resolution. It can be seen that under this resolution, the performance with 1 GHz guard band is quite poor and 1×10^{-3} cannot be

realized. Note that only one network node is considered in the simulation, and in a network configuration with more than one network node, it is expected that the performance would be further degraded and 1-GHz guard band may not result in satisfying performance. One option to solve this problem is to increase the guard band (e.g. to 2 GHz). The alternative method is to reduce the filter resolution. The former is at the expense of the net capacity while the latter imposes design and manufacturing challenge to the HSR filter. Figure 4.4 shows the performance versus the bandwidth of the HSR filter when the resolution is changed to (a) 2 GHz, (b) 1.5 GHz and (c) 1 GHz, when the guard band between channels is 2 GHz. It can be clearly seen that when the resolution of the HSR filter reduces, the tolerance filter bandwidth to obtain the optimal balance among these three channels is relaxed gradually. For 1-GHz resolution, a filter bandwidth between 12 GHz and 13 GHz can obtain the near optimal performance for all channels.

In Figure 4.5, we depict the performance versus the received OSNR for different filter resolution and guard band. The HSR filter bandwidth and the electrical receiver filter bandwidth are optimized for all cases. Clearly, the performance improves as the resolution becomes finer and the guard band increases. When 1-GHz guard band is applied, error floor is observed even when the resolution is reduced to 1 GHz. By increasing the guard band to 2 GHz, no error floor is observed. However, when the resolution is 2 GHz, there are penalties for the added channel 4 and channel 5 due to the crosstalk at the network node. This crosstalk decreases for finer resolution values. Under optimized system parameters, we can see that negligible penalty can be realized when 2-GHz guard band and 1-GHz filter resolution are used.

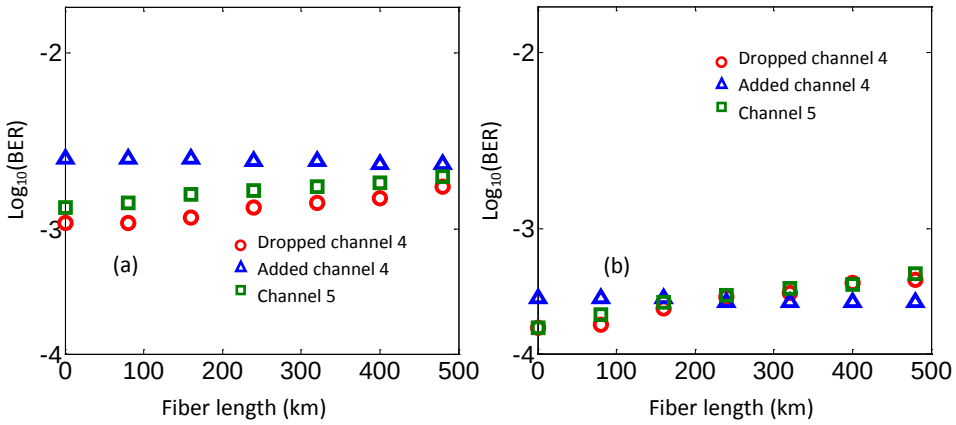

Figure 4.6 – Performance versus the fiber length before the network node when the fiber link after the network node is 0 km. (a) 1-GHz guard band and (b) 2-GHz guard band. The filter resolution is 1 GHz and the OSNR is 12.5 dB per channel. The GI length is 12.

Figure 4.5 is based on the study that the transmission links before and after the networks node have 0-km fiber. To study the transmission effect, Figure 4.6 depicts the performance versus the fiber length before the network node when the fiber link after the network node is 0-km. The OSNR per channel is 12.5 dB and 1-GHz filter resolution is used. The guard interval length is 12 samples. In principle, OFDM is robust to dispersion provided that the guard interval is long enough to overcome intersymbol interference. 12-sample guard interval is sufficient for 500-km fiber dispersion, so it can be seen in the figure that the BER is not very sensitive to the transmission distance before the network node. For the dropped channel (channel 4) and channel 5, the BER increases slightly when the transmission distance increases from 0-km to 480-km transmission. For the added channel, the fiber length before the network nodes does not influence its performance so the BER is kept constant. Figure 4.7 further investigates the transmission performance when the fiber link after the network node is 480 km. For the dropped channel, the performance of Figure 4.7 is similar to that in Figure 4.6 since the 480-km fiber after the network node does not influence the dropped channel. For the added channel, the BERs are higher than that in Figure 4.6 because they are obtained after 480-km transmission (after the network

node). These BERs are constant and do not depend on fiber length before the network node. On the other hand, channel 5 experiences a total transmission distance from 480 km to 960 km when the fiber length before the network node increases from 0 km to 480 km in Figure 4.7. Consequently, not only a BER penalty at 0 km is observed when compared to Figure 4.8 but also the BER degrades gradually as distance increases.

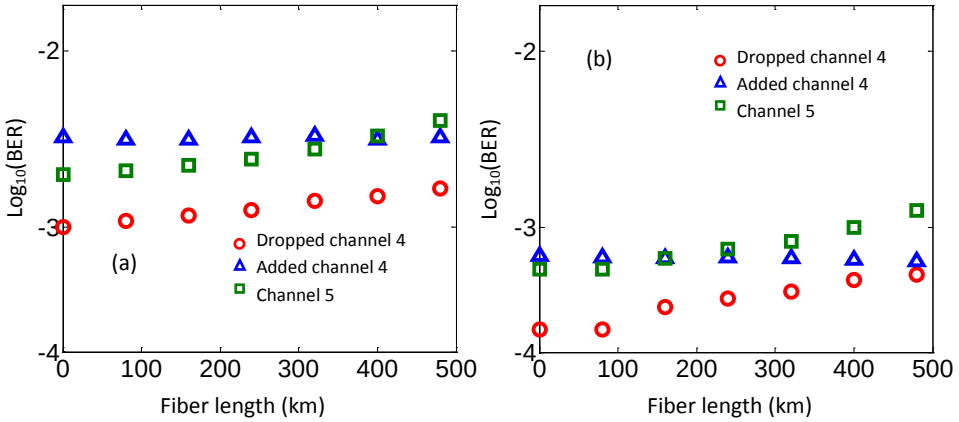

Figure 4.7 – Performance versus the fiber length before the network node when the fiber link after the network node is 480 km. (a) 1-GHz guard band and (b) 2-GHz guard band. The filter resolution is 1 GHz and the OSNR is 12.5 dB per channel. The GI length is 12.

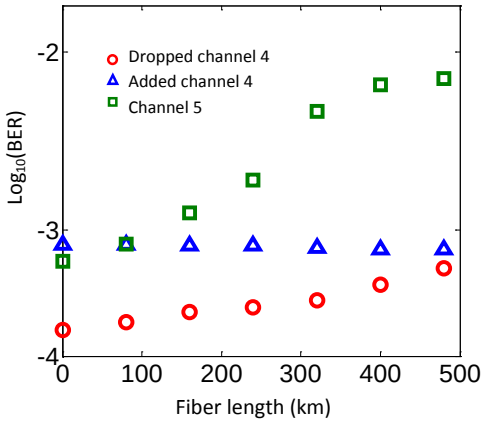

Figure 4.8 – Performance versus the fiber length before the network node for a GI length of 6 when the fiber link after the network node is 480 km. Guard band is 2 GHz and the filter resolution is 1 GHz. The OSNR is 12.5 dB per channel.

Figure 4.6 and Figure 4.7 are based on a guard interval length of 12. As discussed in the transceiver design. The GI length should be sufficient to overcome the dispersion. Figure 4.8 and Figure 4.9 depict the performance versus the fiber length before the network node when the GI length is reduced to 6 and 0 respectively. The fiber length after the network node is 480 km. It can be seen that when the GI length is not sufficient, the performance is degraded significantly. Channel 5 is the most sensitive to the dispersion because this channel experiences the longest transmission reach (the fiber length before the network node + 480 km after the network node). The dropped channel 4 can still maintain the stable performance for a GI length of 6 because this length can be still acceptable to support up to 480 km. However, when the GI length is reduced to 0, as illustrated in Figure 4.9, the performance is also degraded significantly. Finally, the added channel 4 does not depend on the transmission length before the network node but it has fundamental performance penalty arising from the 480 km after the

network node and this penalty is constant and large especially for a GI length of 0 as shown in Figure 4.9.

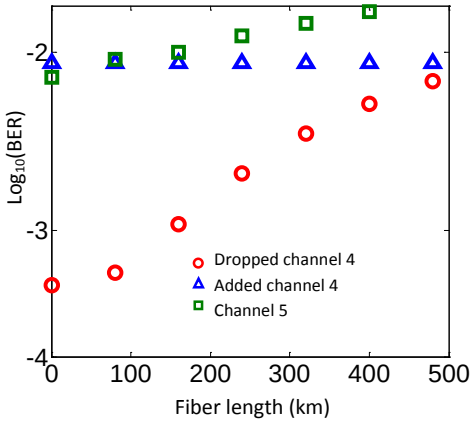

Figure 4.9 – Performance versus the fiber length before the network node for a GI length of 0 when the fiber link after the network node is 480 km. Guard band is 2-GHz and the filter resolution is 1 GHz. The OSNR is 12.5 dB per channel.

4.1.2 HSR filter based node performance for eFOFDM signals

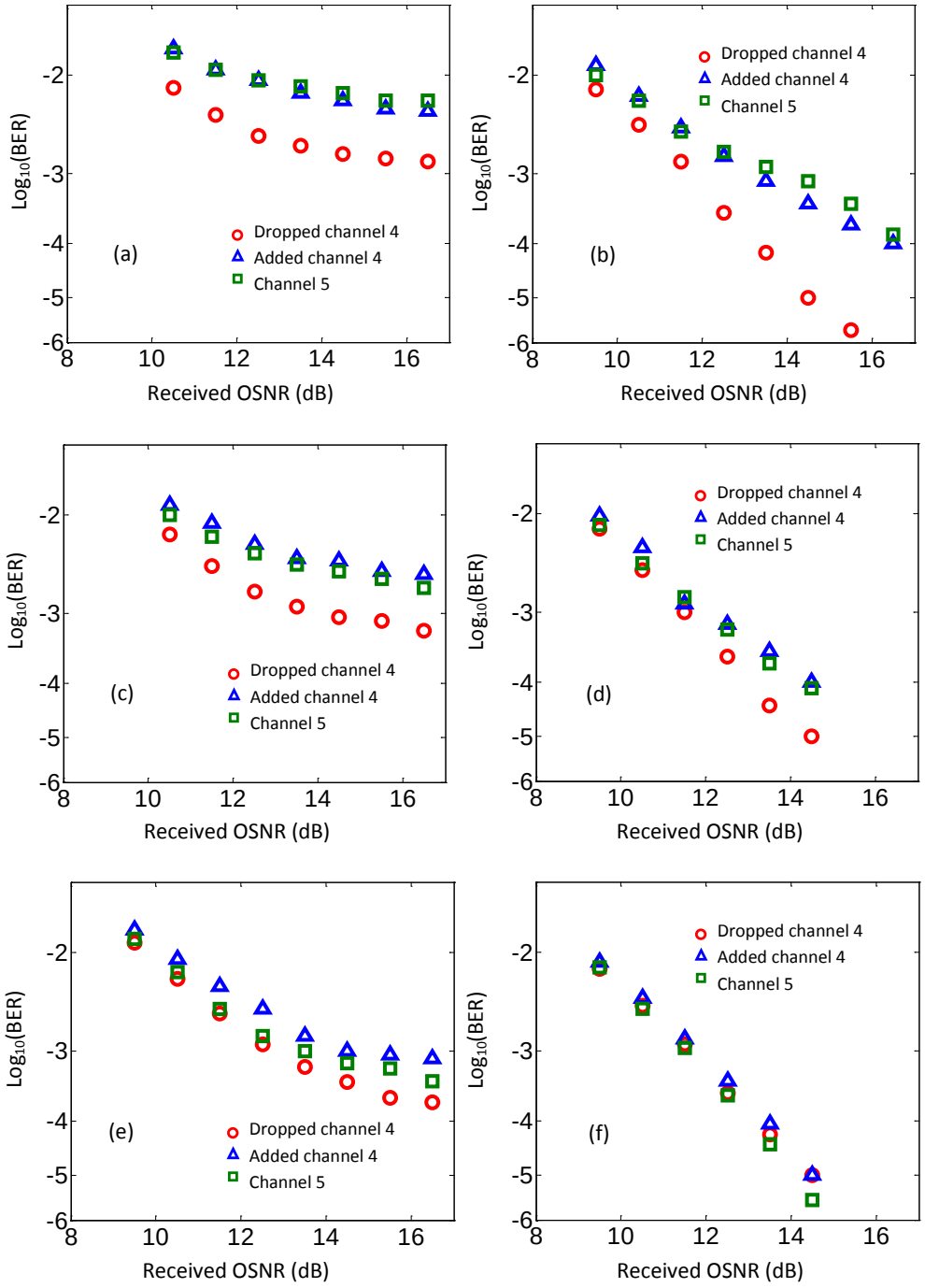

Figure 4.10 – Performance versus the received OSNR (a) 1-GHz guard band and 2-GHz resolution; (b) 2-GHz guard band and 2-GHz resolution; (c) 1-GHz guard band and 1.5-GHz resolution; (d) 2-GHz guard band and 1.5-GHz resolution; (e) 1-GHz guard band and 1-GHz resolution, and (f) 2-GHz guard band and 1-GHz resolution.

The model of the eFOFDM super-channel is the same as that of the conventional OFDM except the DSP procedures. In this subsection, we assume that 8th-order Gaussian-shaped aliasing filter is used with the bandwidth of 6.25 GHz. The HSR filter bandwidth is 12 GHz and the receiver electrical filter bandwidth is 3 GHz. Figure 4.10 depicts the performance versus the received OSNR for different filter resolution and guard band. Similar to conventional OFDM super-channel, when 1-GHz guard band is applied, error floor is observed even when the resolution is reduced to 1 GHz. By increasing the guard band to 2 GHz, no error floor is observed. However, when the resolution is 2 GHz, there are penalties for

the added channel 4 and channel 5 due to the crosstalk induced at the networks node. This crosstalk decreases for finer resolutions. Under optimized system parameters, we can see that negligible penalty can be realized when 2-GHz guard band and 1-GHz filter resolution is used.

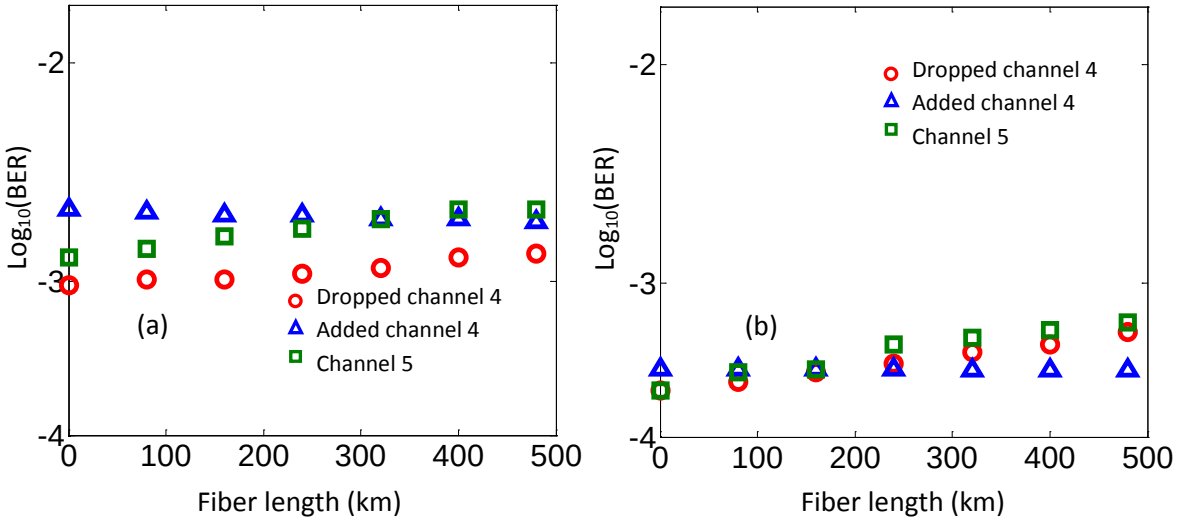

Figure 4.11 – Performance versus the fiber length before the network node when the length after the network node is 0 km. (a) 1-GHz and (b) 2-GHz guard band. The filter resolution is 1 GHz and the OSNR is 12.5 dB per channel. The GI length is 12.

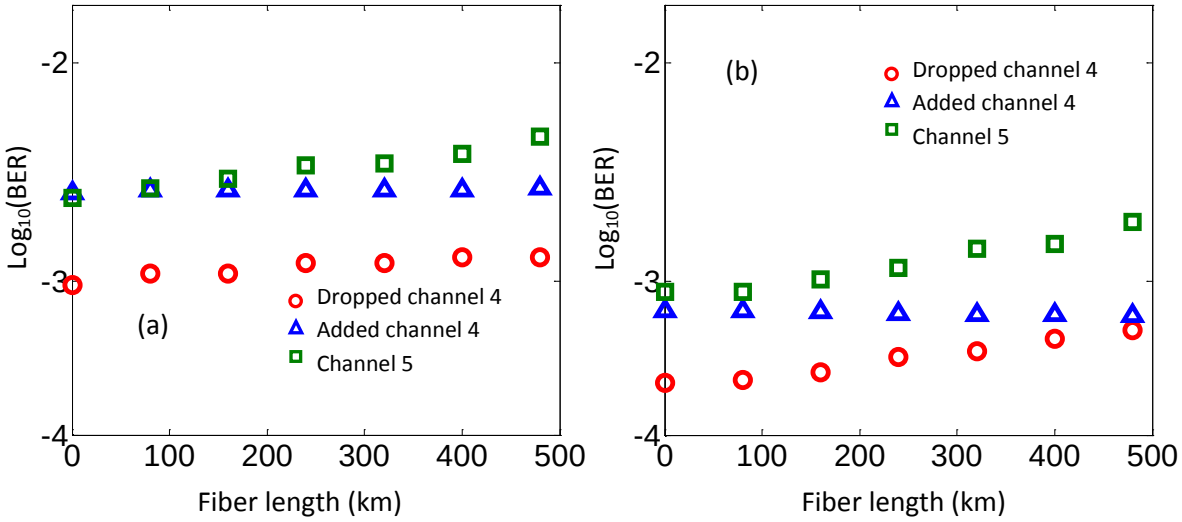

Figure 4.12 – Performance versus the fiber length before the network node when the fiber link after the network node is 480 km. (a) 1-GHz and (b) 2-GHz guard band. The filter resolution is 1 GHz and the OSNR is 12.5 dB. The GI length is 12.

Figure 4.11 depicts the performance versus the fiber length before the network node when the fiber link after the network node is 0 km. The OSNR per channel is 12.5 dB and 1-GHz filter resolution is used. The guard interval length is 12 samples. Similar to conventional OFDM, eFOFDM is robust to dispersion although the design of the guard interval is different from that of the conventional OFDM. Consequently, the BER is not very sensitive to the transmission distance provided that the guard interval length is sufficiently long. For the dropped channel (channel 4) and channel 5, the BER increases slightly when the transmission distance increases from 0 km to 480 km. For the added channel, the fiber length before the network nodes does not influence its performance so the BER is kept constant. Figure 4.12 shows the BER versus the fiber length before the network node when the fiber link after the network

node is 480 km. From both Figure 4.11 and Figure 4.12, we can conclude that the performance of eFOFDM super-channel is similar to that of the conventional OFDM super-channel in terms of the filtering effect in the network nodes. The main difference between eOFDM and eFOFM is on the transceiver side where they have different requirement on the frequency offset, synchronization, and implementation complexity.

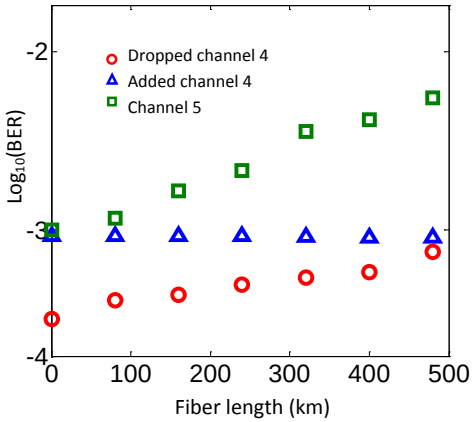

Figure 4.13 – Performance versus the fiber length before the network node for a GI length of 6 when the fiber link after the network node is 480 km. Guard band is 2-GHz and the filter resolution is 1 GHz. The OSNR is 12.5 dB per channel.

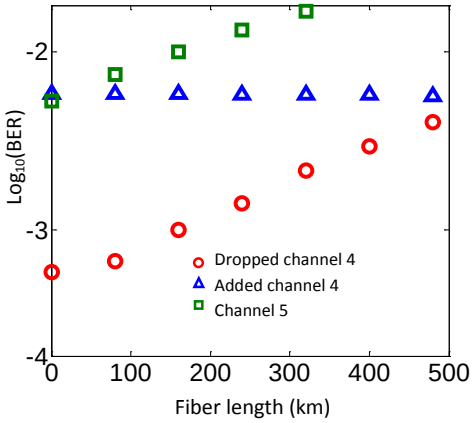

Figure 4.14 – Performance versus the fiber length before the network node for a GI length of 0 when the fiber link after the network node is 480 km. Guard band is 2-GHz and the filter resolution is 1 GHz. The OSNR is 12.5 dB per channel.

Similar to conventional OFDM, eFOFDM based super-channel also requires guard interval to enable dispersion compensation although symmetric rather than cyclic extension based guard interval should be used. The length of the guard interval should be sufficient. Figure 4.13 shows the performance versus the fiber length before the network node when the GI length is reduced from 12 to 6. The length after the network node is 480 km. The filter resolution is 1 GHz and the guard band between channels is 2 GHz. By comparing Figure 4.12 and Figure 4.13, we can see that the performance of all investigated channels is degraded. The dropped channel only experiences the fiber length before the network node (up to 480 km) so we can observe slight performance penalty because a 6-GI length can still be acceptable for this distance. However, for the channel 5, the total transmission distance can be up to 960 km and consequently significant performance penalty is observed. In Figure 4.14, the GI length is reduced to zero. We can see that the performance is further degraded when compared to Figure 4.13 and transmission with BER lower than 10^{-3} cannot be achieved.

As was discussed in Section 0, eOFDM and eFOFDM based super-channel schemes are simpler in the DSP implementation with better back-to-back performance than NFDM based super-channels. However, both schemes require a guard interval to enable dispersion compensation. In contrast, because the spectra of channels do not overlap in NFDM, guard interval is not required, as will be investigated in the next subsection.

4.1.3 HSR filter based node performance for NFDM signals

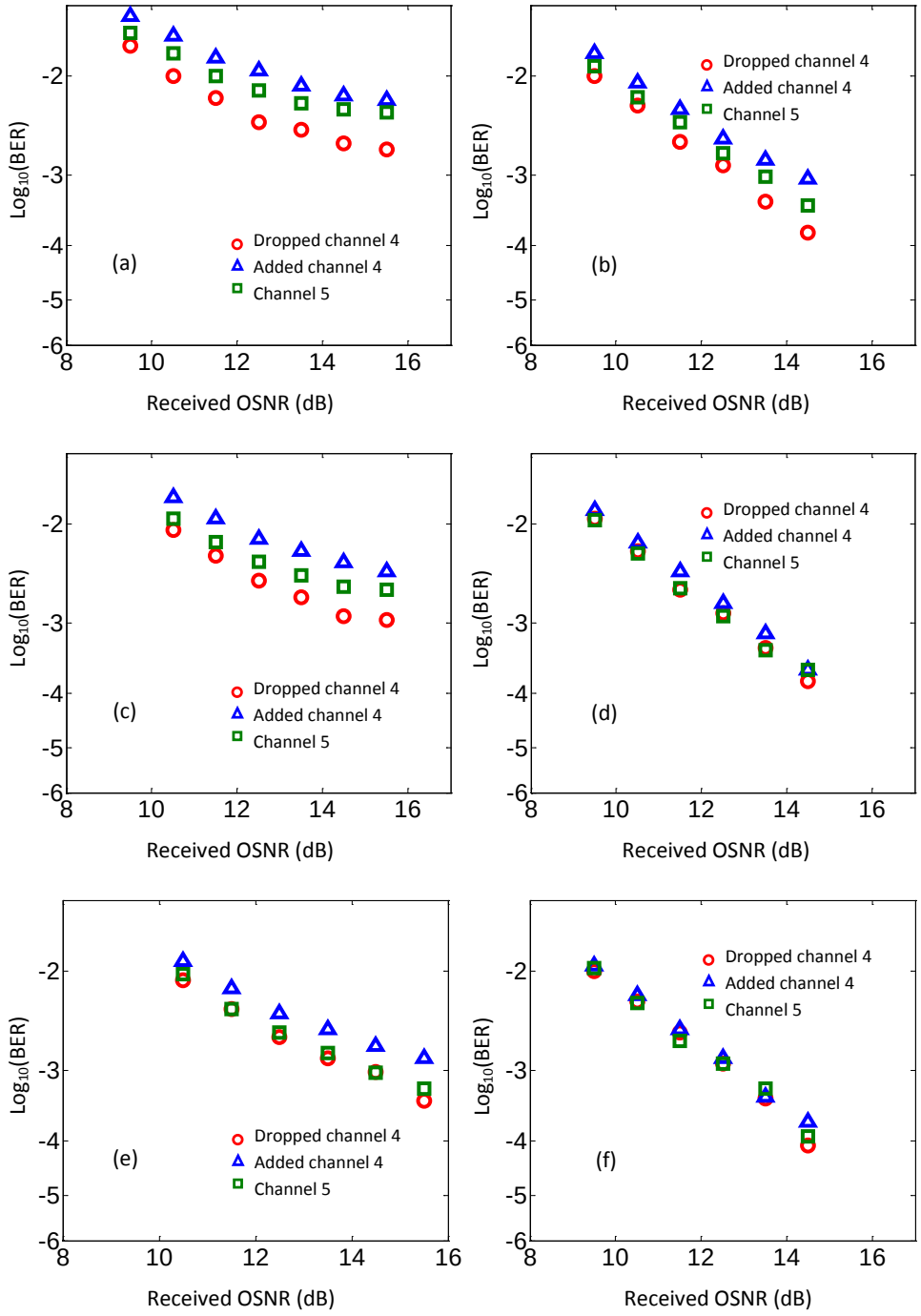

Figure 4.15 – Performance versus the received OSNR (a) 1-GHz guard band and 2-GHz resolution; (b) 2-GHz guard band and 2-GHz resolution; (c) 1-GHz guard band and 1.5-GHz resolution; (d) 2-GHz guard band and 1.5-GHz resolution; (e) 1-GHz guard band and 1-GHz resolution, and (f) 2-GHz guard band and 1-GHz resolution.

Figure 4.15 shows the performance versus the received OSNR under different guard band and filter resolution for NFDM superchannels. Similar to conventional OFDM and eFOFDM, the best performance is obtained for wide guard band and fine filter resolution. It is noted that the performance of NFDM is worse when compared to the OFDM and eFOFDM super-channels. It is because a FIR filter is required to create the rectangular spectrum. In theory, the filter should have infinite memory length. In practice, even with a memory length of 40, which is used in the simulation, the spectral profile is still not ideal and residual crosstalk exists. On the other hand, the advantage of NFDM is that the spectrum of

different subcarriers does not overlap so a guard interval is not required for dispersion compensation. Figure 4.16 and Figure 4.17 show the performance versus the fiber length before the network node when the fiber link after the network node is 0 km (Figure 4.16) and 480 km (Figure 4.17). The OSNR is 12.5 dB per channel. In both figures, the length of guard interval is zero. It can be seen that the performance is still stable even when the guard interval is not used and the performance trend is similar to conventional OFDM and eFOFDM. However, it is noted that the back-to-back penalty exists which hinder NFDM based optical super-channel for high performance applications.

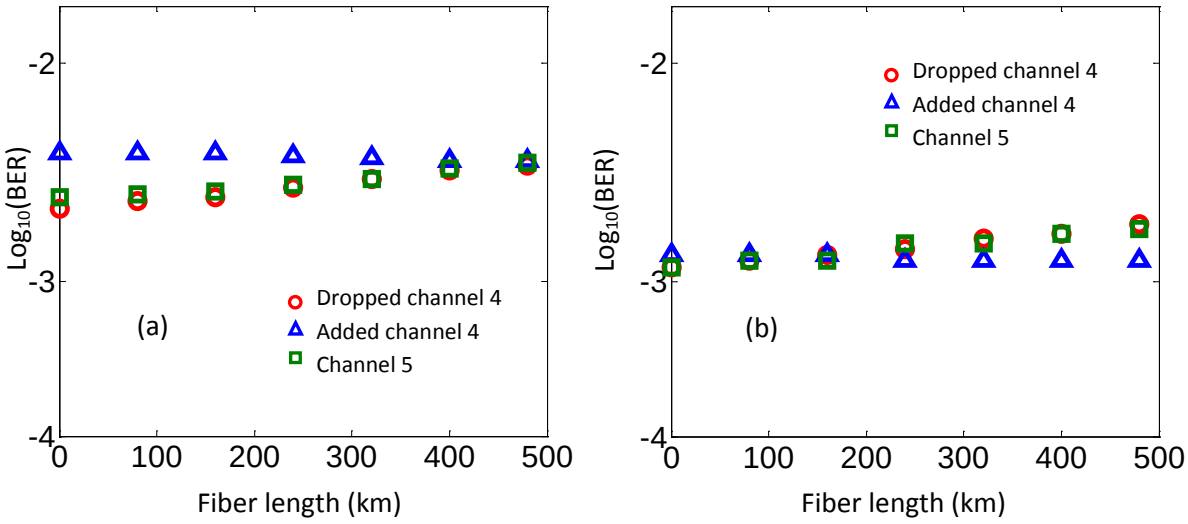

Figure 4.16 – Performance versus the fiber length before the network node when the fiber link after the network node is 0 km. (a) 1-GHz guard band and (b) 2-GHz guard band. The filter resolution is 1 GHz. The GI length is 0.

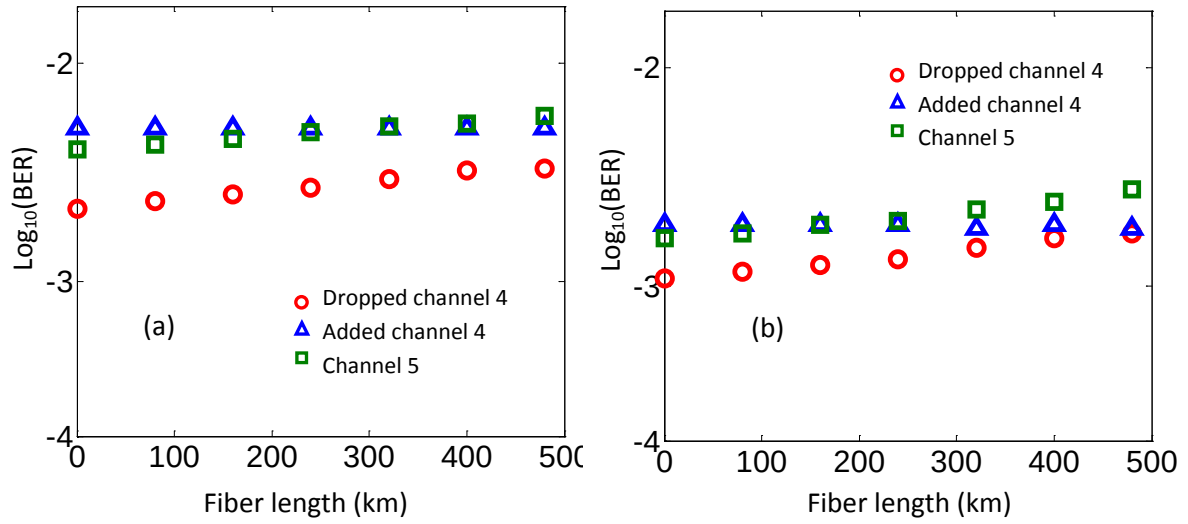

Figure 4.17 – Performance versus the fiber length before the network node when the fiber link after the network node is 480 km. (a) 1-GHz guard band and (b) 2-GHz guard band. The filter resolution is 1 GHz and the OSNR is 12.5 dB per channel. The GI length is 0.

4.2 Performance comparison and discussion

In this chapter, we have investigated the back-to-back performance of the HSR-filter-based node with add and drop capabilities in combination with the transceiver designs for eOFDM, eFOFDM and N-FDM when a seven-channel super-channel generated at the transmitter is filtered at the FOADM node to drop the middle flex-channel (4^{th} channel), and another flex-channel with the same central frequency is added to the super-channel. A study of the performance of the network node when the effect of the transmission is taken into account was also carried out. A comparative table of the BER results obtained for the dropped 4^{th} flex-channel, the added 4^{th} flex-channel and the 5^{th} flex-channel (considering the worst BER per channel, in such a way that the transmission of all three channels can be guaranteed) with each of the transceiver schemes is shown in Table 4.1 and Table 4.2.

In both tables only the results for super-channels with guard band between flex-channels of 2 GHz are shown. With a guard band of 1 GHz, error floor was observed and it was impossible to achieve a BER below 10^{-3} for the three channels under study unless the HSR filter resolution was increased to 1 GHz. In that case, a BER below 10^{-3} is obtained for a received OSNR ≥ 16 dB with eOFDM and eFOFDM, as was shown in Figure 4.5(d) and Figure 4.10(d).

Table 4.1 – Summary of results of back-to-back performance studies carried out for the HSR filter described in section 3.1. Shown are results for a 2-GHz guard band between flex-channels, HSR filter bandwidth of 12 GHz, 2-GHz HSR filter resolution and OSNR = 12.5 dB (unless otherwise stated). Where it says "applicable", it means that the result obtained for the eOFDM case is applicable to the cases of eFOFDM and N-FDM.

BER vs.	eOFDM	eFOFDM	N-FDM
Transceiver + node design (without transmission)			
Tx aliasing filter order	BER slightly higher than 10^{-3} for added 4^{th} ch w/ order ≥ 6 (Figure 4.2)	*(applicable)*	*(applicable)*
Rx electrical filter bandwidth	BER slightly higher than 10^{-3} for added 4^{th} channel w/ BW ~ 3 GHz (Figure 4.3)	*(applicable)*	*(applicable)*
HSR filter bandwidth [*compare with Rx OBPF bandwidth in* Table 2.5]	BER < 10^{-3} for 1-GHz HSR resolution w/ BW ~ 11.5-13.5 GHz BER < 10^{-3} for 1.5-GHz res. w/ BW ~ 11.7-13 GHz BER slightly higher than 10^{-3} for 2-GHz res. w/ BW ~ 12 GHz (Figure 4.1, Figure 4.4)	*(applicable)*	*(applicable)*
Rx OSNR	BER < 10^{-3} for 1-GHz HSR res. w/ OSNR ≥ 11.5 dB, for 1.5-GHz res. w/ OSNR ≥ 12 dB, for 2-GHz res. w/ OSNR ≥ 13 dB (Figure 4.5)	BER < 10^{-3} for 1-GHz & 1.5-GHz HSR res. w/ OSNR ≥ 12 dB, for 2-GHz res. w/ OSNR ≥ 14 dB (Figure 4.10)	BER < 10^{-3} for 1-GHz & 1.5-GHz HSR res. w/ OSNR ≥ 13 dB, for 2-GHz res. w/ OSNR ≥ 14.5 dB (Figure 4.15)

N-FDM incurs a performance penalty compared to eOFDM and eFOFDM in all cases, as can be inferred from the BER vs received OSNR comparison in Table 4.1, as well as from the results of the transmission studies presented in Table 4.2. The eOFDM solution shows the best performance of all three technologies, even though N-FDM achieves a lower and more stable BER when compared to eOFDM and eFOFDM with guard interval lengths of 0 or even 6 samples. However, this improvement comes at the cost of additional filtering in the DSP implementation.

Table 4.2 – Summary of results of transmission performance studies carried out for the HSR filter described in section 3.1. Shown are results for a 2-GHz guard band between flex-channels, OSNR = 12.5 dB and 1-GHz HSR filter resolution with different fibre lengths (L) and guard interval lengths (GI).

BER vs.			**eOFDM**	**eFOFDM**	**N-FDM**
Transmission effect					
L before node when:	*L* after node = 0; GI = 12 samples		BER < $10^{-3.4}$ for up to 480 km (Figure 4.6)	BER < $10^{-3.2}$ for up to 480 km (Figure 4.11)	Stable BER slightly above 10^{-3} for all distances (GI length = 0) (Figure 4.16)
	L after node = 480 km	GI = 12 samples	BER < 10^{-3} for up to 400 km (Ch5 limits performance) (Figure 4.7)	BER < 10^{-3} for up to 150 km (Ch5 limits performance) (Figure 4.12)	Stable BER slightly above 10^{-3} for all distances (GI length = 0) (Figure 4.17)
		GI = 6 samples	BER < 10^{-3} for up to 125 km (Ch5 limits performance) (Figure 4.8)	BER = 10^{-3} for 0 km (Figure 4.13)	
		GI = 0	BER > 10^{-3} (Figure 4.9)	BER > 10^{-3} (Figure 4.14)	

5 Conclusions and remarks

This document reported on the results arising from the development of a system model based on the transmitter-receiver designs analysed in T3.2 and T3.3 and the switching node implementations investigated in T4.1 and T4.2. Two all-optical (AO-OFDM and N-WDM) and three electrical multiplexing schemes (eOFDM, eFOFDM and N-FDM) with 16QAM modulation format were taken into consideration. The back-to-back performance of a single optical channel and a seven-channel super-channel generated and detected by each of the electronic transceiver solutions was evaluated. These formats have similar hardware set-ups regarding the transmitter and receiver implementations, but differ in the DSP encoding and decoding algorithms. The results showed that N-FDM incurred a performance penalty with respect to eOFDM and eFOFDM on account of the very long tails of the sinc function and the impossibility to accomplish a sufficiently sharp roll-off even with large FIR filter memory lengths. However, NFDM has the advantage of non-overlapping channel spectra, which makes the use of a guard interval between channels unnecessary for dispersion compensation.

In the FOX-C project, two switching levels have been considered. At the fibre link level, a WSS selects a super-channel that contains the channels to be dropped locally. At the super-channel level, a filtering technology with ultra-fine granularity is used to separate the closely spaced (or even overlapping) channels. Two filter models have been proposed at the super-channel level: a high resolution filter for non-overlapping channels such as those generated by N-FDM transceivers and an all-optical interferometric filter for overlapping channels such as those generated by AO-OFDM transceivers. In this document we examined the system tolerances imposed by a network node based on the first filter model (HSR) as a function of the transmission and switching impairments. The study took into account that the central channel of a super-channel composed of seven channels would be dropped at the add-drop node and another channel at the same frequency would be added at the same node. It also considered the performance of an adjacent channel travelling from transmitter to receiver. The results showed that it was this channel that usually limited the transmission performance of the system.

From the results of the transmission studies carried out for the HSR filter, it was also observed that, for an OSNR = 12.5 dB, a 2-GHz guard band between flex-channels, a 1-GHz HSR filter resolution and a guard interval length of 12 samples would be required to guarantee a reasonable performance of a super-channel based on eOFDM and eFOFDM. N-FDM showed a back-to-back performance penalty that caused the BER to be above 10^{-3} in all cases. However, N-FDM achieved a lower and more stable BER when compared to eOFDM and eFOFDM with guard interval lengths of 0 or even 6 samples.

Finally, it is noteworthy that the system modelling studies whose results were presented in this document offer a powerful and accurate tool for the overall system performance evaluation studies in T2.3, which will aim at the identification of the operating limits of a flexible network and the benefits of such a network in terms of power consumption and cost saving.

References

1. S.L. Jansen, I. Morita, T.C.W. Schenk, N. Takeda, and H. Tanaka, "Coherent optical 25.8Gb/s OFDM transmission over 4160km SSMF," IEEE Journal of Lightwave Technology **26**, 6-15 (2008).

2. Q. Yang, Z. He, Z. Yang, S. Yu, X. Yi, and W. Shieh, "Coherent optical DFT-spread OFDM transmission using orthogonal band multiplexing," Opt. Express **20**, 2379-2385 (2012).

3. X. Liu and F. Buchali, "Intra-symbol frequency-domain averaging based channel estimation for coherent optical OFDM," Optics Express **16**, 21944-21957 (2008).

4. B. Liu, L. Zhang, X. Xin, and J. Yu, "None pilot-tone and training sequence assisted OFDM technology based on multiple-differential amplitude phase shift keying," Opt. Express **20**, 22878-22885 (2012).

5. W. Shieh, H. Bao, and Y. Tang, "Coherent optical OFDM: theory and design," Opt. Express **16**, 841-859 (2008).

6. B. Inan, S. Adhikari, O. Karakaya, P. Kainzmaier, M. Mocker, H. V. Kirchbauer, N. Hanik, and S. L. Jansen, "Real-time 93.8-Gb/s polarization-multiplexed OFDM transmitter with 1024-point IFFT," Opt. Express **19**, B64-B68 (2011).

7. J. Zhao and A. D. Ellis, "A novel optical fast OFDM with reduced channel spacing equal to half of the symbol rate per carrier," in Optical Fiber Communication Conference, paper OMR1, 2010.

8. J. Zhao and A. D. Ellis, "Advantage of optical fast OFDM over OFDM in residual frequency offset compensation," IEEE Photon. Technol. Lett. **24**, 2284-2287 (2012).

9. J. Zhao and H. Shams, "Fast dispersion estimation in coherent optical 16QAM fast OFDM systems," Opt. Express **21**, 2500-2505 (2013).

10. J. Zhao and A. D. Ellis, "Transmission of 4-ASK optical fast OFDM with chromatic dispersion compensation," IEEE Photon. Technol. Lett. 24, 34–36 (2012).

11. R. Schmogrow, D. Hillerkuss, M. Dreschmann, M. Huebner, M. Winter, J. Meyer, et al., "Real-Time Software-Defined Multiformat Transmitter Generating 64QAM at 28 GBd," Photonics Technology Letters, IEEE **22**, 1601-1603 (2010).

12. R. Schmogrow, S. Wolf, B. Baeuerle, D. Hillerkuss, B. Nebendahl, C. Koos, et al., "Nyquist frequency division multiplexing for optical communications," in Lasers and Electro-Optics (CLEO), 2012 Conference on, pp. 1-2, 2012.

13. R. M. Schmogrow, M. Meyer, P. C. Schindler, A. Josten, S. Ben-Ezra, C. Koos, et al., "252 Gbit/s Real-Time Nyquist Pulse Generation by Reducing the Oversampling Factor to 1.33," in Optical Fiber Communication Conference/National Fiber Optic Engineers Conference 2013, Anaheim, California, paper. OTu2I.1, 2013

14. D. M. Marom, et al., "Wavelength-selective 1×K switches using free-space optics and MEMS micromirrors: theory, design, and implementation," J. Lightwave Technol. **23**, 1620-1630 (2005).

15. Kelly, J., "Application of liquid crystal technology to telecommunication devices," National Fiber Optic Engineers Conference (NFOEC), 2007.

16. M.A.F. Roelens et al, "Dispersion trimming in a reconfigurable wavelength selective switch," IEEE J. Lightwave Technol **26**, 73-78 (2008).

17. D. Sinefeld, and D. M. Marom, "Colorless photonic spectral processor using hybrid guided-wave/free-space optics arrangement and LCoS modulator," Optical Fiber Communication (OFC) 2009.